(NASA-CR-164640) PRECIPITATION GROWTH IN CONVECTIVE CLOUDS Final Technical Report, 1 Aug. 1979 - 31 Jul. 1981 (Chicago Univ.) 52 p HC A04/MF A01 CSCL 04B

N81-28667

Unclas
G3/47 27055

Final Technical Report

NASA NSG 5402

PRECIPITATION GROWTH IN CONVECTIVE CLOUDS.

PRECIPITATION GROWTH IN CONVECTIVE CLOUDS

FINAL REPORT

Principal Investigator: R.C. Srivastava

Period Covered: August 1, 1979 to July 31, 1981

Grantee Institution: The University of Chicago
5801 South Ellis Avenue
Chicago, Illinois 60637

Grant Number: NSG - 5402

1. Introduction:

Several investigations were carried out. In the following I shall give: a list of publications, highlights of the findings, and research in progress not yet written up for publication.

2. Publications:

The research resulted in the following papers which have been submitted for publication:

a: Robinson, W.D., and R.C. Srivastava, 1981: Calculations of Hailstone Growth in a Sloping Steady Updraft. Submitted to Atmosphere - Ocean. Also LAP TR #44 .

b: Srivastava, R.C., 1981: A Simple Model of Particle Coalescence and Breakup. Submitted to the Journal of Atmospheric Sciences. Also LAP TR #44.

c: Matejka, T.J. and R.C. Srivastava, 1981: Doppler Radar Study of a Region of Widespread Precipitation Trailing a Mid-Latitude Squall Line. To appear in the Preprints of the 20th Conference on Radar Meteorology. (A more detailed paper will also be submitted for journal publication.) Also LAP TN #10.

It may be mentioned that most of the work for (a) was done under an NSF grant. The NASA grant provided the opportunity and support for organizing the results of the research and writing it up for journal publication. The work for (b) was supported by NASA and NSF. The data collection on which (c) is based was supported by NSF; NASA and NSF provided support for the data analysis and research.

3. Results

Full details of the results of the investigations may be found in the above papers (copies attached). In the following I shall summarize the main results and their significance.

3.1 Hail Growth;

Sustained falls of large hail are usually associated with clouds having a sloping updraft which can be regarded as quasi-steady. A number of studies have demonstrated that the trajectory of the growing hail is important in considerations of hail growth and artificial modification of hail processes.

A simple model of a sloping updraft and hail growth was set up for which analytical solutions could be obtained. It was found that the starting position of the hail embryo has an important effect on its subsequent growth. Three regions of embryo starting positions were distinguished. Embryos starting in the central portions of the updraft are carried up rapidly and displaced far from the updraft into the anvil. Most of these particles cannot survive during fall to the ground. Embryos starting near the upshear edge of the updraft have a simple arcing up and down trajectory and produce hailstones most of which can be expected to melt before reaching the ground. Embryos starting in the third region, namely, the region near the downshear edge of the updraft give rise to the largest hailstones and have predominantly re-circulating trajectories.

It is believed that the subject deserves further study; an investigation of the general properties of particle trajectories in model flow fields can give insights into hail growth processes which will be difficult, if not impossible, to obtain from numerical models.

3.2 Particle Coalescence and Breakup

The processes of particle coalescence and breakup, spontaneous and collisional, are important in determining the evolution of particle size spectra. A firm understanding of the evolution of particle sizes is important for a number of reasons: The particle size distribution is involved in various methods for measuring precipitation rates and in numerical studies of cloud dynamics.

Previous studies have identified, to some extent, the roles of the various processes in shaping particle size spectra. Coalescence tends to produce particles of larger sizes and exponential spectra of the kind observed in nature. Coalescence and breakup tend to produce stationary exponential distributions. The effects of collisional disintegration dominate over those of spontaneous disintegration as the precipitation content increases, and the equilibrium spectra tend to be parallel to each other.

The above findings from numerical models are verified by analytical solutions of the kinetic equation for the particle size distribution for simplified forms of the collection and breakup functions in paper (b). The exact analytical solutions provide insights into the processes governing the forms of particle size spectra not available from numerical calculations.

3.3 Precipitation Associated with a Squall Line

During PROJECT NIMROD, extensive Doppler radar observations of squall lines were obtained in Illinois. Paper (c) discusses observations of a region of widespread precipitation trailing a squall line. Such regions of widespread precipitation are often observed in association with mid-latitude squall lines and more generally in the case of tropical squall lines. Physical considerations suggest that the region of widespread precipitation may have meso-scale vertical motions in it which could be important dynamically as well as for budgets of various quantities. An important budget quantity is the rainfall. It is often observed that while the intense rain associated with the convective cores of a squall line is relatively spotty and short-lived, the light rain associated with the region of wide-spread cloudiness last for a long time and extends over a much larger area. It has been estimated that the precipitation associated with the region of widespread cloudiness often contributes a significant fraction (≈ 0.5) of the total precipitation from the squall line system. This also supports the idea that vertical motions exist in the region of widespread precipitation.

In paper (c), we have extended the VAD method to obtain accurate estimates of small vertical motions ($w \simeq 10$ cm s^{-1}) and applied it to observations of widespread precipitation associated with a squall line system. The results show generally ascending motions in the upper parts of the cloud and descending motions in the lower parts of the cloud. It is suggested that precipitation evaporation associated with the descent, and precipitation production associated with the ascent help maintain the observed vertical air motions.

4. Research in Progress

Work discussed in 3.3 is continuing. We anticipate obtaining quantitative estimates of the rain output from the squall line system using data from a dense network of raingauges (average spacing $\simeq$ 3 km).

5. Copies of the papers mentioned in Section 2 are attached.

Calculations of Hailstone Growth

in a Sloping Steady Updraft

by

W. D. Robinson* and R. C. Srivastava

Department of Geophysical Sciences
The University of Chicago
Chicago, Illinois 60637

*Present affiliation: Computer Sciences Corporation, Washington, D.C.

Abstract

Analytical solutions to the equations of growth and motion of hailstones in updrafts and cloud water contents which vary linearly with height are used to investigate hail growth in a model cloud. The model storm is steady and two-dimensional and is constructed by compositing sections with linear variations of vertical air velocity and cloud water content so as to approximate the Fleming storm. Hail embryos are introduced at various positions in the updraft and their subsequent history calculated. A strong correlation is found between the embryo starting position and its trajectory and final size. Embryos starting in the central portions of the updraft are carried up rapidly and displaced far from the updraft. Embryos starting near the upshear edge of the updraft have a simple arcing up and down trajectory and produce small hailstones which can be expected to melt before reaching the ground. Embryos starting near the downshear edge of the updraft give rise to the largest hailstones and have predominantly recirculating trajectories. Effects of changing some of the model parameters are investigated.

I. INTRODUCTION

The foundations of the theory of hail growth were laid by Schumann (1938) and Ludlam (1958). Ludlam showed that the requirement of heat-balance does not always allow all the water accreted by a hailstone to freeze. In Ludlam's model, the excess (unfrozen) water was shed; this limited the maximum size to which a hailstone could grow to a diameter of about 4 cm. However, experiments by List (1959) showed that the unfrozen water need not be shed from the growing hailstone but rather that the hailstone can grow in a "spongy" mode. By assuming that no water is shed from a growing hailstone, Hitschfeld and Douglas (1963) showed that large hailstones can grow in a one-dimensional (vertical) cloud, in times consistent with observations, provided high concentrations of water are present as postulated by Marshall (1961). In their work on hail growth, Sulakvelidze et al. (1967) also considered regions of high water content or accumulation zones.

Building on the above pioneering work, and spurred by possible application to artificial modification of hail, a considerable volume of research on hail growth has been reported in the recent literature. The simplest models of hail growth are one-dimensional models in which the vertical air velocity and cloud microphysical properties are prescribed functions of height or height and time. (e.g. List et al., 1968; Musil, 1970; and Dennis and Musil, 1973). A somewhat more complex but still a one-dimensional model of hail growth considers interacting dynamics and microphysics (e.g., Wisner et al., 1972 and Danielsen et al., 1972).

A criticism of one-dimensional models is that the storm dynamics are not adequately modeled or simulated in one dimension. Further, observations show that, at least in middle latitudes, storms producing sustained large hail occur in an environment having a vertical shear of the horizontal wind, suggesting that the horizontal dimension plays an important role in the hail process. This has been stressed by Ludlam (1963) and others.

Calculations of hail growth in two-dimensional models were reported by English (1973), Orville and Kopp (1977) and others. Guided by certain observed characteristics of Alberta hailstorms, English prescribed the vertical air velocity and water content as functions of vertical and horizontal distance, and showed that hail of observed sizes could be grown in the clouds in reasonable times. The liquid fraction of the hailstones grown in the model were reasonable and not excessive as in the one-dimensional model of Hitschfeld and Douglas. Orville and Kopp considered a two-dimensional model with highly parameterized microphysics. It is doubtful that the dynamics are properly simulated in two dimensions and the calculation of hail growth suffers because of the extensive parameterization of microphysics. However, the simplifications of two-dimensionality and the microphysical parameterizations were dictated by computer limitations.

It appears that the dynamics, microphysics and the horizontal and vertical dimensions all are important in the problem of sustained falls of large hail. A detailed numerical calculation considering all the parameters cannot be performed on present-day computers. Also it is doubtful that such a calculation would be very illuminating. Therefore, qualitative models based on physical considerations and observations become important. Among such models, we mention those of Browning (1963, 1964, 1977) and Browning and Foote (1976) which clearly demonstrate that both the vertical and the horizontal dimensions are important in the process of hail growth.

In this paper, we present a two-dimensional, steady-state model of hail growth in a sloping updraft which is simplified to the point that analytical solutions for hailstone growth and trajectory become possible. In spite of its simplicity, the model illustrates the effects of particle trajectory on its growth and reproduces certain aspects of the qualitative models mentioned in the previous paragraph. The model used here is an extension of the two-dimensional model of precipitation growth in an upright axially-symmetric steady-state updraft presented by Srivastava and Atlas (1969). Other two- and three-dimensional models which compute hail or precipitation particle trajectory and growth are those of English (1973), Sartor and Cannon (1976) and Paluch (1978).

2. THE MODEL

We consider a steady-state two-dimensional model of a storm. The model storm consists of a number of "sections" in the horizontal and the vertical in each of which the vertical air velocity and the "effective" cloud water content are linear or piece-wise linear functions of the height and constant in the horizontal direction. Discontinuous changes in certain parameters are permitted between horizontal sections. These assumptions allow analytical solutions to be obtained for the particle size and position. We shall now present the equations for the model.

2.1 Equations

The following equations apply to a portion of the model cloud in which the cloud properties vary linearly with height and are constant in the horizontal. Details of some of the derivations can be found in Srivastava and Atlas (1969).

The vertical air velocity is given by

$$w = w_o + \alpha z \tag{1}$$

where w_o and α are constants and z is the vertical coordinate. The "effective" liquid water content for hail growth is considered to be the product of M, the cloud water content, and E, the collection efficiency of hail; we assume

$$ME = \gamma_o + \gamma_1 z \tag{2}$$

where γ_o and γ_1 are constants. The terminal velocity V of hail of diameter D is taken as

$$V^2 = KD \tag{3}$$

where K ($\cong 2 \times 10^6$ cm s^{-2}) is a constant. This should be acceptable for D $\gtrsim$ 1 mm. The continuous collection equation for hail growth is

$$\frac{dD}{dt} = \frac{ME}{2\rho} V \tag{4}$$

where ρ (taken as 0.9 g cm^{-3}), is the density of the hailstone. It is assumed that no water is shed from the hailstone. A weakness of this model is that the liquid fraction of the hailstone is not calculated. The vertical position of the particle is given by:

$$\frac{dz}{dt} = w - V \quad . \tag{5}$$

The above equations can be combined to yield the following equation for the z and V of a growing particle:

$$\frac{d^2z}{dt^2} - \alpha \frac{dz}{dt} + \beta_1 z = -\beta_o \tag{6}$$

$$\frac{d^2V}{dt^2} - \alpha \frac{dV}{dt} + \beta_1 V = \beta_1 w_o - \alpha\beta_o \tag{7}$$

where

$$\beta_o = \frac{K}{4\rho} \gamma_o \quad , \quad \beta_1 = \frac{K}{4\rho} \gamma_1 \tag{8}$$

are constants. Analytical solutions for the above second order linear differential equations with constant coefficients can be easily obtained.

We now consider the horizontal position x of the particle. It is given by

$$\frac{dx}{dt} = u \tag{9}$$

where u is the horizontal velocity. For slab symmetry u is given by

$$\rho_a \frac{\partial u}{\partial z} + \frac{\partial (\rho_a w)}{\partial z} = 0 \quad . \tag{10}$$

The air density ρ_a is assumed to be

$$\rho_a = \rho_o \exp(-\lambda z) \tag{11}$$

where λ is a constant, we take

$$\lambda = \left(\frac{g}{R} - \bar{\gamma} \right) / \bar{T} \tag{12}$$

where g is the acceleration due to gravity, R is the gas constant for air and $\bar{\gamma}$ the mean lapse rate of temperature and $\bar{T}$ the mean temperature. From the above equations, we have

$$\frac{dx}{dt} = x \cdot [\lambda w - \alpha] \tag{13}$$

The above equation can be integrated to give the trajectory of an air particle starting at (x_o, z_o)

$$x = x_o \cdot \frac{w_o + \alpha z_o}{w_o + \alpha z} \cdot \exp[\lambda(z - z_o)] \tag{14}$$

and the position of a growing hail particle

$$x = x_o \exp[(\lambda w_o \alpha - \alpha - \frac{\lambda\beta_o\alpha}{\beta_1})t + \frac{\lambda\alpha}{\beta_1}(V-V_o)] \quad , \beta_1 \neq 0$$

$$x_o = x_o \exp[\frac{\lambda\beta_o t^2}{2} + (\lambda V_o - \alpha)t + \lambda(z-z_o)] \quad , \quad \beta_1 = 0 \qquad (15)$$

where V_o is the initial fall speed of the particle at (x_o, z_o).

The solution of (6), (7) and (15) gives the particle fall speed and vertical and horizontal positions in terms of the initial conditions (V_o, x_o, z_o) and the model parameters $(w_o, \alpha, \beta_o, \beta_1, \lambda)$.

2.2 Model Composition

The cloud described in the equations of Section 2.1 does not have enough flexibility to model realistic sloping updrafts. The airflow to the right of the plane of symmetry of such a model is shown schematically in Fig. 1. At the lower levels, air converges inward and at the higher levels, the air diverges outward into the anvil. By appropriately piecing together portions of the model of fig. 1, with other portions of this model, or portions of models with different parameters, it is possible to approximate fairly general sloping updrafts. Thus we can take the portion ABCD of fig. 1 and join it with a portion from a different model at the top or the sides, and continue the process to get a composite model. Certain constraints must be observed in this compositing process. Continuity of mass must be considered at the interfaces. The streamlines (Eq. 14) are such that no air crosses them. Thus the choice of left and right edges of a section is the streamline at the edge. It can be seen from Eqn. (14) that the streamlines do not change if w_o/α remains constant. Thus sections

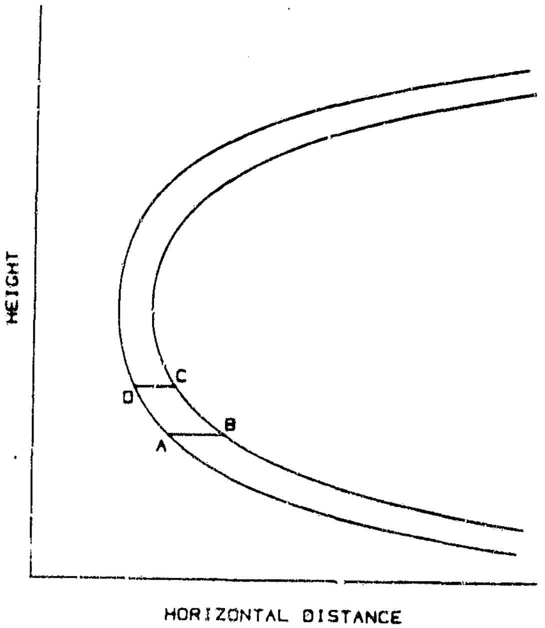

Figure 1.
Schematic air particle trajectories in a slab symmetric cloud.

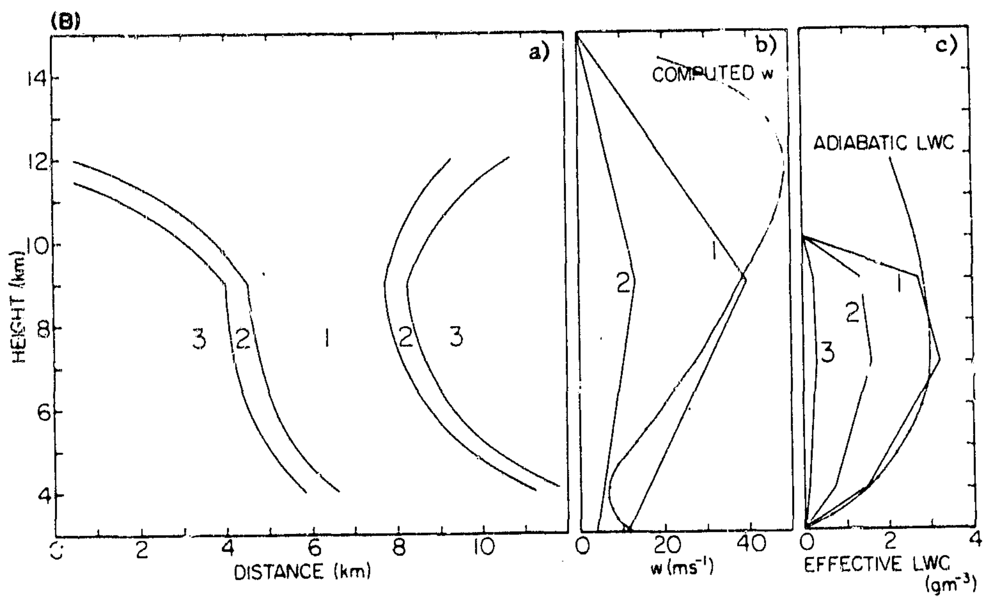

Figure 2. (a) The updraft shape, and the distributions of (b) vertical air velocity and (c) effective cloud water content in the model Fleming storm.

can be placed side by side if they have the same value of w_o/α. Still air sections have no streamline constraints. In piecing sections vertically, we require continuity of mass flux. The vertical mass flux through a horizontal boundary is wL, where L is the length of the horizontal boundary. In this model, vertically adjacent sections have the same L; thus the vertical velocity is required to be continuous at the horizontal interfaces between sections.

2.3 Model parameters

The parameters of the model storm will be selected to approximate the quasi-steady-state phase of the Fleming Storm (Browning and Foote, 1976). The model storm consists of three adjacent sections (Fig. 2). The updraft velocity in the three sections is shown by the correspondingly numbered curves in Fig. 2b. Section 3 is composed of still air. Section 2 is a transition region between the core of the updraft, Section 1, and the still air section. The vertical velocity in Section 2 is 1/3 of that in Section 1. In each of the sections, the updraft and effective liquid water content are piecewise linear functions of the vertical coordinate and constant in the horizontal. The vertical air velocity in the core of the updraft near the cloud base is 11.2 m s^{-1} and is comparable to the vertical air velocity measured by instrumented aircraft near the base of the Fleming cloud. The vertical velocity in the model is zero near the observed top of the Fleming cloud. No measurements of the vertical air velocity were available in the body of the Fleming cloud. Using parcel theory (with no water loading) the temperature sounding data yielded the updraft shown by the continuous curve. The model updraft assumes a lower maximum vertical air velocity located near the middle of the cloud rather than near the cloud top. According to Sulakvelide et al. (1967) and Marwitz (1972), the maximum vertical air velocity occurs in the middle levels of cloud.

The assumed effective liquid water content in the model cloud (fig. 2c) is an approximation to the computed adiabatic effective liquid water content (continuous curve) except at the higher levels. The sharp cutoff at the higher levels is due to the reduced collection efficiency of hail because of glaciation. No collection takes place above the level of the -40C isotherm (10 km).

The slope of the updraft corresponds roughly to what is known about the Fleming storm (cf. fig. 11 of Browning and Foote). The width of the updraft at cloud base is taken as 8 km (core width - 6 km). At a height of 9 km, the model updraft narrows to about half its width at the cloud base.

3. CALCULATIONS AND RESULTS

Hailstones are initiated on embryos of diameter 0.1 cm. The embryos are placed inside the updraft with even spacing in the vertical and horizontal of 1 and 1/2 km respectively. The embryo placement covers the height range from 5 to 10 km; the latter is the height of the -40C isotherm while embryos of the assumed size are considered unlikely to occur below the former height. The growth and motion of the embryos is followed using analytical solutions of the equations given in Section 2. More embryos are subsequently placed in regions requiring greater resolution. During the computations embryos which move out of the computational box (fig. 2a) are excluded from further consideration and are designated "out of cloud particles."

3.1 Results for the model Fleming storm

Some representative hailstone trajectories are shown in fig. 3. Of the 57 evenly spaced embryos, 38 fall out of the computational box; thus 2/3 of the embryos are designated "out of cloud." Most of these particles grow only for a short time in their upward trajectory before entering the no-growth region above 10 km height and being expelled from the computational box (e.g. trajectory 2 in fig. 3). A similar feature can also be seen in Robertson's model (Robertson, 1975). The final diameters (at 0C level) of these particles are less than 0.3 cm. The starting region of these embryos is indicated by the shading in Fig. 4.

Ten of the 19 embryos, which fall inside the computational box, display a simple arcing up and down trajectory (e.g. trajectory 1, fig. 3). These particles start to the left of the shaded "out of cloud" region (see fig. 4). None of these particles attained a diameter greater than 0.5 cm at the 0C level. These particles should melt completely before reaching the ground. The growth time of these particles is about 10 to 20 minutes (shown by the full curves in fig. 4).

Hail of diameter about 1 cm and larger originates on embryos which start in a narrow region on the right side of the updraft (trajectories 3 and 4, fig. 3). This region is small; it contains only 9 of the 57 embryos. Most of the embryos starting in this region execute one or more recirculations. The number of recirculations increases as the embryo starting position approaches the right edge of the updraft, and the particles with the largest number of recirculations start at the 9 km height, which is the height at which the updraft turns over. Many of the particles spend over half of their time in the recirculation region and grow to half their

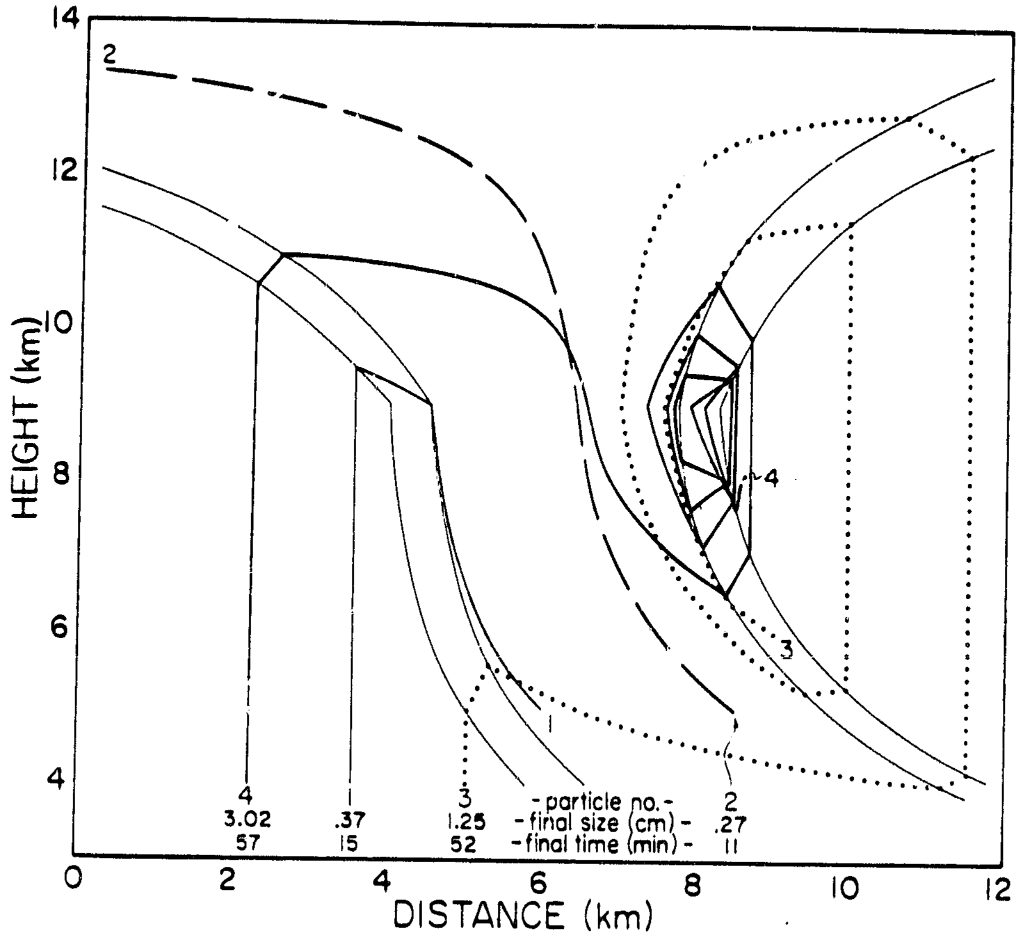

Figure 3. Representative particle trajectories in the model Fleming storm. The diameter and elapsed time (both at the OC level) are indicated.

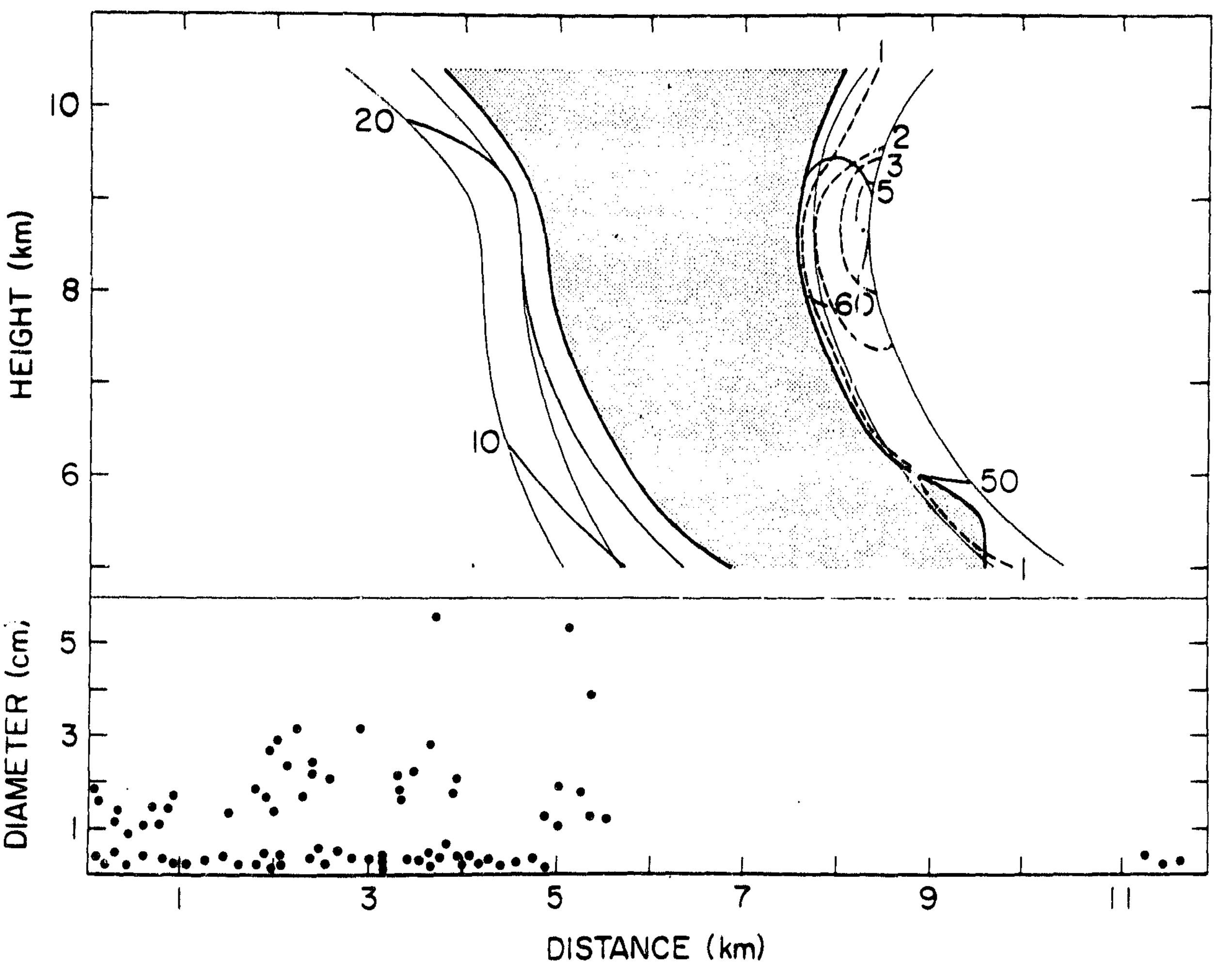

Figure 4. (Top) Contours (dashed) of hail diameter, cm, and elapsed time, minutes (solid). (Bottom) Fall-out location and diameter of hailstone. The diameter and time refer to the OC level.

final size there. The final diameters of these particles range between 1.7 and 5.7 cm, and the growth times range between 40 and 60 minutes (see fig. 4). The maximum size (5.7 cm diameter) is in good agreement with the baseball size hailstones reported for the Fleming storm during its quasi-steady phase lasting over 3 hrs.

Histograms of final diameters at the OC level and elapsed times (fig. 5) show the number of embryos producing the hail of indicated size and the time taken for the hail to reach that level. The elapsed time histogram shows a bimodal distribution; the low mode is composed of embryos originating on the left side of the updraft while the high mode is due to the particles originating on the right side of the updraft. The final diameter histogram is similar to the elapsed time histogram. A large fraction of the embryos produce hail of diameter less than 1 cm. These embryos start on the left side of the updraft. There is a drop in particle number around 1 cm diameter and then a lower peak occurs. This peak is due to embryos starting on the right side of the updraft.

An interesting correlation was found between the fall-out location and the final diameter of the hail. The major portion of the hailfall begins about 2 km behind the updraft with exclusively large hail. The largest hail size decreases with increasing distance behind the updraft edge (see bottom portion of fig. 4). Figure 4 (bottom) also shows a tendency for hail of diameter greater than 1 cm to bunch together into groups behind the updraft. The bunching persisted even when the embryos were distributed with a finer spacing. It is possible that the bunching is an intrinsic property of particle sorting

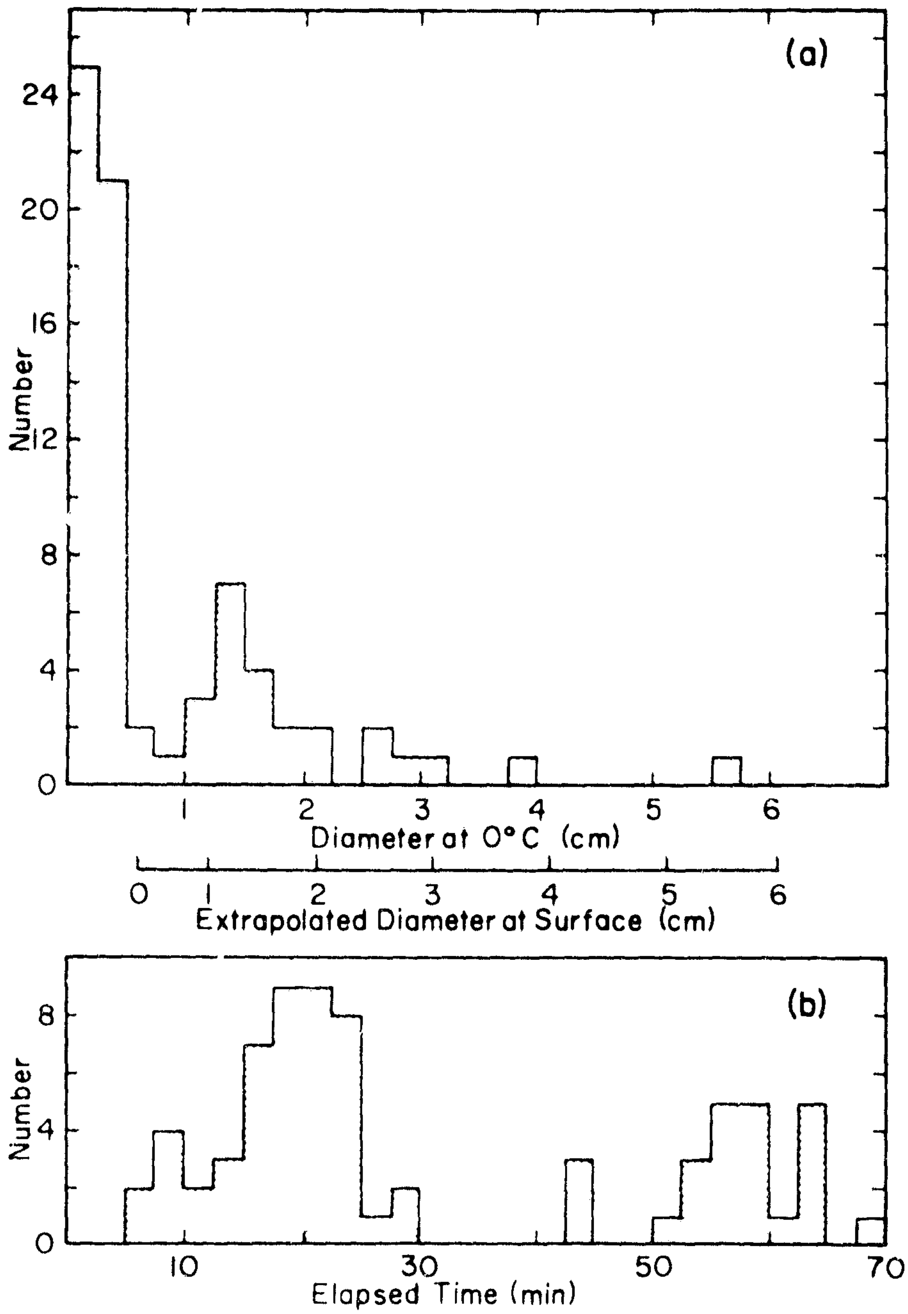

Figure 5. (a) Relative numbers of embryos (initially, uniformly distributed over the updraft, see text) and their final diameters. (b) relative numbers of embryos and elapsed time. The diameters and times refer to the OC level.

in patterns of sloping updrafts. With a moving storm, the bunching could perhaps give rise to a streaky pattern of hail fall at the ground. Towery and Morgan (1977) and others have reported streaky patterns of hail at the ground.

3.2 Variations on the model Fleming storm

To test the sensitivity of the results to the model input we repeated the calculations changing the values of some of the parameters. In the results presented in figs. 6 and 7, the model is similar to the model Fleming storm, except that the maximum vertical air velocity has been reduced from 40 m s^{-1} to 30 m s^{-1} and 20 m s^{-1} respectively.

The case with the maximum vertical velocity of 30 m s^{-1} is similar in many respects to the model Fleming case. However, the region of the updraft contributing to "out-of-cloud" particles decreases. The maximum hailstone size does not change significantly. The case with the 20 m s^{-1} maximum vertical air velocity has a much smaller "out-of-cloud" region. This case has a recirculation-mode region which gives rise to large hailstones as in the case of the model Fleming storm. But it also shows another region from which large hailstones originate. This region is on the right side of the updraft near its base and yields hailstones with maximum diameter of about 4 cm in about 25 minutes. The trajectories of embryos starting in this region is an up, across and down arc with a small loop. The hailstones are able to balance in the high liquid water content region and grow rapidly. This case also yields 1 cm diameter hailstones in 15 minutes and 2 cm diameter stones in 20 minutes via arcing trajectories. The results for this case bear a great deal of resemblance to the results of Paluch (1978).

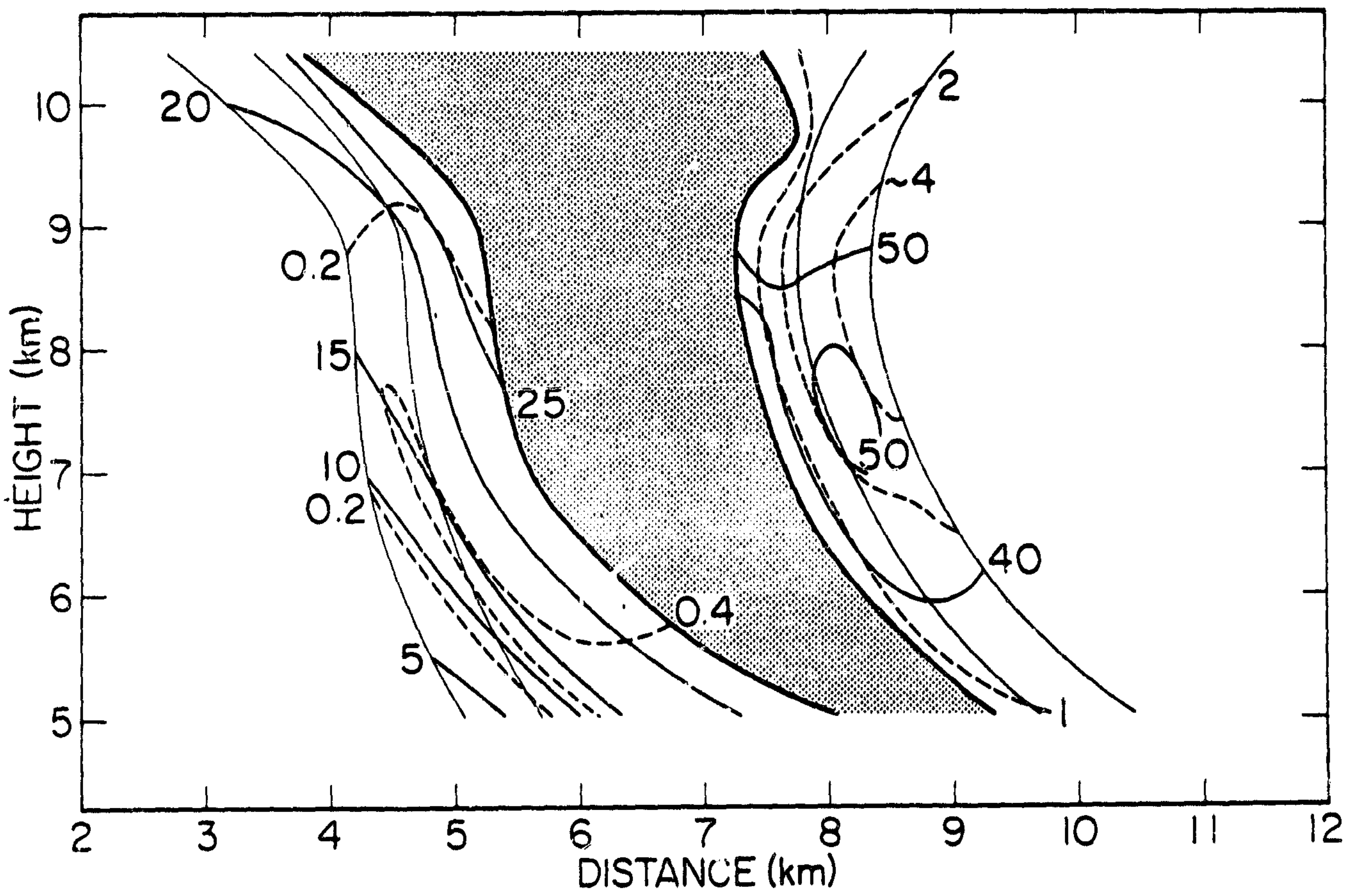

Figure 6. Similar to Fig. 4 but with the maximum vertical air velocity reduced to 30 m s^{-1}.

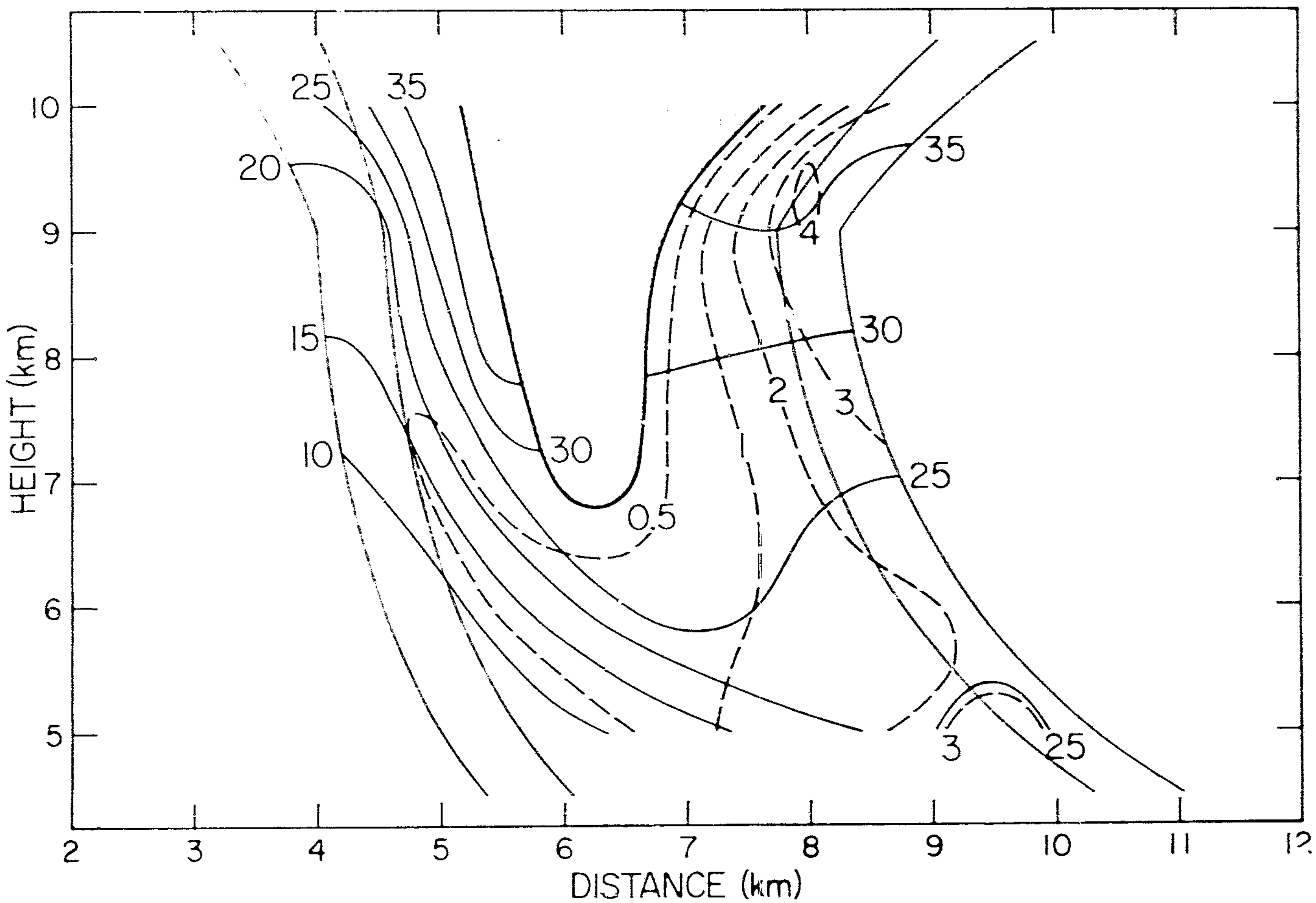

Figure 7. Similar to Fig. 4 but with the maximum vertical air velocity reduced to 20 m s^{-1}.

A calculation was also performed by changing the width of the updraft of the model Fleming storm from 8 km to 6 km (the width of the transition region was kept the same). In this case, the elapsed time for trajectories was similar to that in the case of the model Fleming storm. However, the maximum hailstone diameter decreased from 5.7 to 3.6 cm. This decrease was due to a decrease in the number of recirculations of hailstones. The general results of this case are similar to those of English (1973).

3.3 Particle trajectories

Three types of particle trajectories have been encountered in the model Fleming storm depending upon the starting position of the embryo. These trajectories are summarized in fig. 8e and compared with the results of Paluch (1978), fig. 8(a) through 8(d). Paluch used three-dimensional motion fields obtained from Doppler radar observations and calculated particle growth and trajectories assuming the motion field to be steady; the microphysical parameters were also prescribed and assumed to be steady. The trajectory types obtained by Paluch (fig. 8a, b, and c) are basically similar to the trajectory types 1, 3 and 4 (fig. 8e) obtained by us. Hence, it appears that our conclusions, for the model Fleming storm, might be applicable more generally to storms with sloping updrafts.

4. SUMMARY AND CONCLUSIONS

Analytical solutions to the equations of growth and motion of hailstones have been obtained for steady-state linear variations of the vertical air velocity and effective cloud water content (product of collection efficiency and cloud water content) with height. Fairly general models of quasi-steady storms with sloping updraft can be constructed by piecing

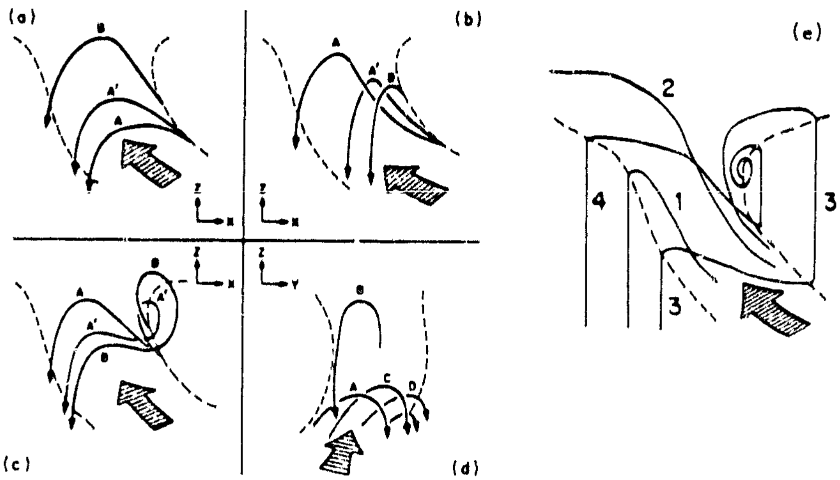

Figure 8. *A summary of particle trajectories obtained by Paluch, 1978 (a, b, c and d), and those obtained here (e). Note that d refers to a plane perpendicular to that of a, b and c.*

together sections with piece-wise linear variations of updraft and effective cloud water content. In this way a model of the Fleming storm has been set up and the growth and motion of hail embryos in the storm computed. Three distinct situations arise depending upon the starting position of the hail embryo. Embryos starting in the middle portion of the updraft travel far from the main updraft and attain only small sizes; most of these hailstones are not expected to survive the fall from the 0C isotherm to the ground. Embryos starting on the upshear edge of the updraft undergo an arcing up, over and down trajectory and give rise to hailstones of diameter less than 0.5 cm; these particles also are not expected to survive the fall from the 0C level. Embryos starting on the downshear edge of the updraft give rise to hail of diameter greater than 1 cm, the maximum diameter being 5.7 cm. These embryos execute recirculations, with the number of recirculations and the final hailstone size increasing with the proximity of the embryo starting position to the turn-over location of the updraft. The existence and location of this region (temperature, vertical air velocity) are believed to be important for the growth of large hail. It is believed that the three types of particle trajectories identified here, and the associated growth patterns would obtain in most cases of quasi-steady sloping updrafts.

Acknowledgments: This research was supported by grants NSF ATM 78-01011 and NASA NSG-5402. Thanks are due to Ms. Gail Barton for her excellent typing of the manuscript.

References

Browning, K.A. (1963) The growth of large hail within a steady updraught. Quart. J. Roy. Meteor. Soc., 89, 490-506.

Browning, K.A. (1964) Airflow and precipitation trajectories within severe local storms which travel to the right of the winds. J. Atmos. Sci., 21, 634-639.

Browning, K.A. (1977) The structure and mechanisms of hailstorms. Hail: A Review of Hail Science and Hail Suppression. G.B. Foote and C.A. Knight, Eds., Meteor. Monogr., No. 38, 1-43.

Browning, K.A. and G.B. Foote (1976) Airflow and hail growth in supercell storms and some implications for hail suppression. Quart. J. Roy. Meteor. Soc., 102, 499-533.

Danielsen, Edwin F., R. Bleck and D.A. Morris (1972) Hail growth by stochastic collection in a cumulus model. J. Atmos. Sci., 29, 135-155.

Dennis, A.S. and D.J. Musil (1973) Calculations of hailstone growth and trajectories in a simple cloud model. J. Atmos. Sci., 30, 278-288.

English, M. (1973) Alberta hailstorms, Part II: Growth of large hail in the storm. Meteor. Monogr. No. 36, Amer. Meteor. Soc., 98 pp.

Hitschfeld, W. and R.H. Douglas (1963) A theory of hail growth based on studies of Alberta storms. Z. Angew. Math. Phys., 14, 554-562.

List, R. (1959) Wachstum von Eis-Wassergemischem im Hagelver Suchskanal. Helv. Phys. Acta, 32, 293-296.

List, R., R.B. Charlton and P.I. Buttuls (1968) A numerical experiment on the growth and feedback mechanisms of hailstones in a one-dimensional steady-state model cloud. J. Atmos. Sci., 25, 1061-1074.

Ludlam, F.H. (1958) The hail problem. Nubila, 1, 1-96.

Ludlam, F.H. (1963) Severe local storms: A review. Meteor. Monogr., 5, no. 27, 1-30, Boston, Amer. Meteor. Soc.

Marshall, J.S. (1961) Inter-relation of the fall speed of rain and the updraft in hail formation. Nubila, 4, 59-62.

Marwitz, J.D. (1972) The structure and motion of severe hailstorms. Part III: Severely sheared storms. J. Atmos. Sci., 11, 189-201.

Musil, Dennis J. (1970) Computer modeling of hailstone growth in feeder clouds. J. Atmos. Sci., 27, 474-482.

Orville, H.D. and Fred J. Kopp (1977) Numerical simulation of the life history of a hailstorm. J. Atmos. Sci., 34, 1596-1618.

Paluch, Ilga R. (1978) Size sorting of hail in a three-dimensional updraft and implications for hail suppression. J. Appl. Met., 17, 763-777.

Robertson, D. (1975) The trajectories of particles growing by accretion of cloud droplets. Sci. Rep. MW-87, Stormy Weather Group, McGill University, 13 pp.

Sartor, J.D. and T.W. Cannon (1977) The observed and computed microstructure of hail-producing clouds in northeastern Colorado. J. Appl. Meteor., 16, 710-714.

Schumann, T.W. (1938) The theory of hailstone formation. Quart. J. Roy. Meteor. Soc., 64, 3-21.

Srivastava, R.C. and D. Atlas (1969) Growth, motion and concentration of precipitation particles in convective storms. J. Atmos. Sci., 26, 535-544.

Sulakvelidze, G.K., H.Sh Bibilashvili, and V.F. Lapcheva (1967) Formation of precipitation and modification of hail processes. Translated by Israel Program for Scientific Translations, Jerusalem, 208 pp.

Towery, N.G. and G.M. Morgan, Jr. (1977) Hailstripes. Bull. Amer. Meteor. Soc., 58, 588-591.

Wisner, Chester, H.D. Orville and Carol Myers (1972) A numerical model of a hail-bearing cloud. J. Atmos. Sci., 29, 1160-1181.

A Simple Model of Particle Coalescence and Breakup

by

R. C. Srivastava

Department of Geophysical Sciences
The University of Chicago
Chicago, Illinois 60637

25 July 1981

ABSTRACT:

A simple model of the evolution of particle size distributions by coalescence and spontaneous and binary disintegrations is formulated. Spontaneous disintegration involves single particles, while coalescence and binary disintegrations involve pairs of particles. Analytical solutions for the mean mass of the distribution and the equilibrium size distribution are obtained for the case of constant collection kernel and disintegration parameters. At equilibrium, the forms of the size distributions are identical under the action of coalescence and either or both disintegration processes; the particle concentration is proportional to the total mass concentration (M) and the mean mass of the distribution is independent of M when only coalescence and binary disintegrations are operative. At small values of M, the effects of spontaneous disintegrations dominate over those of binary disintegrations while the reverse is the case at large values of M. Some of the findings of the present simple model are in qualitative agreement with the results of numerical calculations of the evolution of raindrop size spectra with realistic formulations of drop coalescence and breakup.

1. INTRODUCTION

Coalescence and breakup are among the important processes governing the evolution of precipitation particle size spectra. Coalescence alone tends to increase the concentration of the larger particles, and decrease that of smaller particles. Particle breakup opposes this tendency of coalescence and it is conceivable that a combination of coalescence and breakup would produce stationary particle size distributions. Indeed this was found to be the case in a number of numerical studies of the evolution of particle size spectra. Srivastava (1971) found equilibrium size spectra resulting from the action of coalescence and spontaneous breakup of raindrops. Studies of coalescence and spontaneous and collisional breakup (e.g. Gillespie and List 1978, Srivastava 1978 and Young 1975) also showed the development of an equilibrium size distribution for raindrops. Furthermore, it was found that: (i) the effect of collisional breakup dominates over that of spontaneous breakup at large precipitation mass contents (M), while the reverse is the case at small M, and (ii) the equilibrium size distributions resulting from coalescence and collisional breakup are parallel to each other, or more explicitly, at equilibrium, the particles concentrations are proportional to M.

In this paper, we set up a simple formulation of particle coalescence and breakup which admits of analytical solutions. These solutions show explicitly the approach to equilibrium and the relative importance of spontaneous and collisional breakup in determining the particle size distributions. The solutions also reproduce qualitatively some of the results found in the numerical calculations cited above.

2. MODEL & EQUATIONS

We consider a discrete size distribution, the particle masses being taken as the integers. The process of coalescence cannot produce particles of non-integral mass. The process of particle breakup will be formulated so that it too cannot produce particles of non-integral mass.

The usual formulation of particle coalescence will be adopted, that is, the rate at which particles of masses j and k combine to increase the concentration of particles of mass (j + k) will be taken as $K(j,k)p_jp_k$, where p_j is the concentration of particles of mass j and K(j,k) is the collection kernel.

Two modes of particle breakup will be considered. First, spontaneous breakup of particles of mass k will be assumed to occur at a rate αp_k, where α, the spontaneous disintegration parameter, can in general be a function of k. The second mode of particle breakup, involving a pair of particles, is similar to collisional breakup and will be referred to as binary breakup. Binary breakup involving particles of masses j and k will be assumed to proceed at a rate βp_jp_k where the binary disintegration parameter β can in general be a (symmetrical) function of j and k. All fragments resulting from disintegrations will be assumed to be of unit size.

The time rate of change of particle concentration is given by

$$\frac{dp_k}{dt} = \frac{1}{2}\sum_{j=1}^{\infty} K(j,k-j)p_{k-j}\, p_j \tag{1a}$$

$$- p_k \sum_{j=1}^{\infty} K(j,k)p_j - \alpha(k)p_k - p_k \sum_{j=1}^{\infty} \beta(j,k)p_j, \quad k \geq 2$$

$$\frac{dp_1}{dt} = - \sum_{j=1}^{\infty} K(1,j)p_1p_j + \sum_{j=2}^{\infty} \alpha(j)jp_j$$

$$+ \frac{1}{2}\sum_{j=1}^{\infty}\sum_{k=1}^{\infty} \beta(j,k)\ (j+k)p_jp_k - p_1 \sum_{j=1}^{\infty} \beta(1,j)p_j \tag{1b}$$

For $k \geq 2$, the first two terms on the right hand side of Equation (1a) represend respectively the rates of gain and loss of particles of size k by coalescence, the third term represents the loss of particles by spontaneous disintegration and the last term represents the rate of loss of particles by binary disintegrations. Equation (1b) gives the rate of change of concentration of particles of unit size. The first term on the right hand side of the equation represents the loss of particles by coalescence. The second term represents the gain in particle concentration by spontaneous breakup, while the third and fourth terms represent the gain by binary disintegrations.

It can be shown that Equations (1) ensure the conservation of total mass concentration

$$M = \sum_{k=1}^{\infty} k p_k \tag{2}$$

in the system provided K and β are symmetric functions of their arguments.

A general solution of equations (1) is not possible. For the coalescence only ($\alpha=\beta=o$) problem, analytical solutions were reported in the literature (e.g. Scott, 1968) for special forms of the collection kernel, namely, a constant kernel, a kernel proportional to the sum of particle masses, a kernel proportional to the product of particle masses, and a kernel which is a linear combination of the three foregoing kernels. In the following, we shall give an analytical solution of Equations (1) for a constant collection kernel K and constant breakup parameters α and β. Other forms of K, and α and β will be briefly considered in Section 4.

3. SOLUTION OF EQUATIONS AND RESULTS

3.1. Constant Kernel and Breakup Parameters

We introduce the generating function

$$G(z,t) = \sum_{k=1}^{\infty} p_k (t) z^k \tag{3}$$

It can be shown that for constant $K(=c)$, α and β, the generating function satisfies:

$$\partial G/\partial t + (cN+\beta N+\alpha)\ G = (c/2)G^2 + M\ (\alpha+\beta N) z \tag{4}$$

where

$$N = N(t) = \sum_{k=1}^{\infty} p_k (t) = G(1,t) \tag{5}$$

is the total particle concentration. The following scaled variables will be used.

$$\begin{aligned}
\tau &= cMt \\
\alpha_* &= \alpha/cM \\
\beta_* &= \beta/c \\
P_k(t) &= p_k(t)/M \\
g(z,t) &= G(z,t)/M = \sum_{k=1}^{\infty} P_k\ (t) z^k
\end{aligned} \tag{6}$$

The mean mass of the distribution m is given by:

$$m\ (t) = M/N(t) = 1/g\ (1,t)\ . \tag{7}$$

If an equilibrium solution results, the equilibrium quantities will be distingushed by a subscript E. In terms of the scaled quantities, Equation (4) may be rewritten as:

$$\partial g/\partial\tau + (\alpha_* + \beta_*/m + 1/m)g = g^2/2 + (\alpha_* + \beta_*/m)z \tag{8}$$

We shall now consider the behavior of the mean mass and the equilibrium particle size distribution.

3.1.1 Mean Mass

Putting z=1 in Eq. (8), we have for the mean mass of the distribution:

$$\frac{dm}{dt} = (1/2 + \beta_*) + (\alpha_* - \beta_*)m - \alpha_* m^2 \tag{9}$$

First, we consider certain special cases. For the case of coalescence only, we have:

$$m\ (\tau) = m\ (o) + \tau/2 \tag{10}$$

Thus the mean mass of the system increases linearly and the concentration tends to vanish with increasing time.

If coalescence and spontaneous breakup are considered, the solution of Equation (9) is

$$y = (y_o + \tanh x)/(1 + y_o \tanh x) \tag{11}$$

where y and x are related to m_o and τ by Equations (15) and (16) repsectively but with $\beta_* = o$. The initial condition is $y = y_o$ at $\tau = o$. It is seen from Equation (11) that as $x \to \infty$, $y \to 1$; thus as $\tau \to \infty$, an equilibrium mean mass is approached which is given by the following equation

$$m_E = 1/2 + (1/4 + 1/2\alpha_*)^{1/2} \tag{12}$$

As might have been anticipated, the equilibrium mean mass decreases with increasing value of the scaled breakup parameter α_*. As $\alpha_* \to \infty$, $m_E \to 1$, that is all particles tend to be of unit size. Equation (12) also implies that for fixed α/c, m_E increases with M. For M large, or more precisely, for

$$cN(o) \quad /2\alpha >> 1, \qquad m_E \cong (c/2\alpha)M^{1/2}$$

It can be shown that the approach to equilibrium takes place monotonically. An example is shown in Fig. 1. In this example $m_E = 215$. For an initial $m(o) = 450$, m_E is approached to within 10% at $\tau = 400$. Coalescence alone would have doubled the mean mass at $\tau = 200$. It can also be shown that the equilibrium is stable, that is, perturbations of m about its equilibrium value tend to return m to the equilibrium value.

If only coalescence and binary disintegration are considered, the solution of (9) is:

$$m(\tau) = m(o)\bar{e}^{\beta_*\tau} + (1 + 1/2\beta_*)(1 - \bar{e}^{\beta_*\tau}) \tag{13}$$

As $\tau \to \infty$, the following equilibrium mean mass is approached:

$$m_E = 1 + 1/2\beta_* = 1 + c/2\beta \tag{14}$$

The equilibrium mean mass tends to 1 as $\beta_* \to \infty$. In contrast to the previous case, m_E is independent of the mass concentration. This suggests that at equilibrium, plots of the size distribution for different mass concentrations will be parallel to each other. This is verified later. It can also be shown that, as in the previous case, the approach to equilibrium is monotonic and the equilibrium is stable.

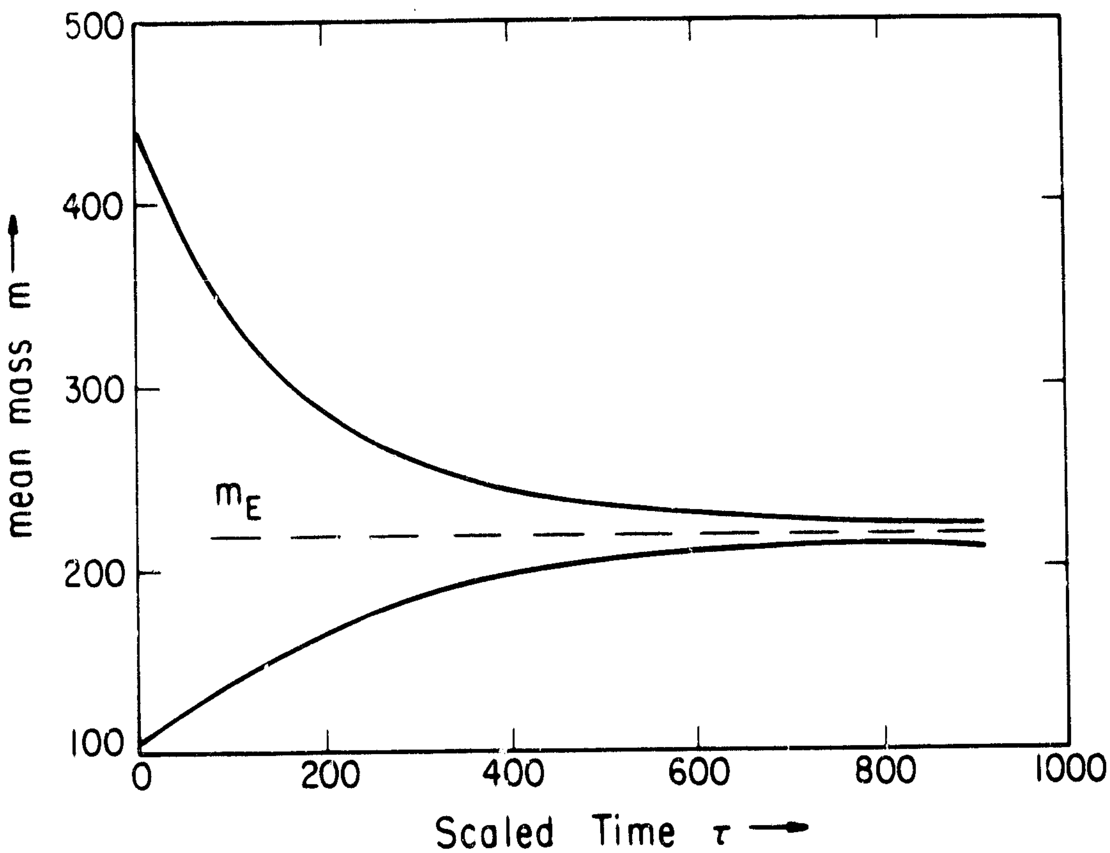

Figure 1. Two examples of the variation of mean mass with scaled time for coalescence and spontaneous and binary breakup ($\alpha_* = 10^{-5}$, $\beta_* = 10^{-4}$).

In the general case of coalescence and spontaneous and binary disintegrations the solution of (9) is given by (11) where y and x are related to m and τ by

$$y = \left(m - \frac{\alpha_*-\beta_*}{2\alpha_*}\right) / \left[(1/2\alpha_* + \beta_*/\alpha_*) + (\alpha_* - \beta_*)^2 / 4\,\alpha_*^2\right]^{1/2} \tag{15}$$

$$x = \tau.\ \alpha_* \left[(1/2\alpha_* + \beta_*/\alpha_*) + (\alpha_* - \beta_*)^2 / 4\alpha_*^2\right]^{1/2} \tag{16}$$

and y_o is the initial value of y. As $\tau \to \infty$, an equilibrium mean mass is approached:

$$m_E = (\alpha_* - \beta_*)/2\alpha_* + \left[(1/2\alpha_* + \beta_*/\alpha_*) + (\alpha_* - \beta_*)^2 / 4\alpha_*^2\right]^{1/2} \tag{17}$$

It may be noted that (12) is a special case of (17), obtained by putting $\beta_* = o$ in the latter. Also the limit of (17) as $\alpha_* \to o$ gives equation (14). Again, it can be shown that the approach to equilibrium is monotonic and the equilibrium is stable.

The behavior of m_E is summarized in Fig. 2. The thin curves show the variation of m_E with α_* for selected β_*. The thick curve shows m_E as a function of β_* for $\alpha_* = o$. It is seen that m_E decreases with increases in both α_* and β_*.

It may be recalled that the scaled spontaneous disintegration parameter α_* (= α_o/cM) involves the mass concentration M. It is perhaps more instructive to consider the behavior of m_E with M for fixed α/c and β/c. This is done in Fig. 3. With coalescence and binary disintegration ($\alpha_* = o$), m_E is independent of M (dotted curve). With coalescence and spontaneous disintegration ($\beta_* = o$), m_E varies approximately as $M^{1/2}$ (dashed curve). The full curve is for coalescence and both types of disintegrations. At samll M, this curve approaches the spontaneous breakup curve, and at large M, it approaches the binary disintegration curve. Thus, at small M, the effect of spontaneous disintegration predominates over the effect of binary disintegrations; as M

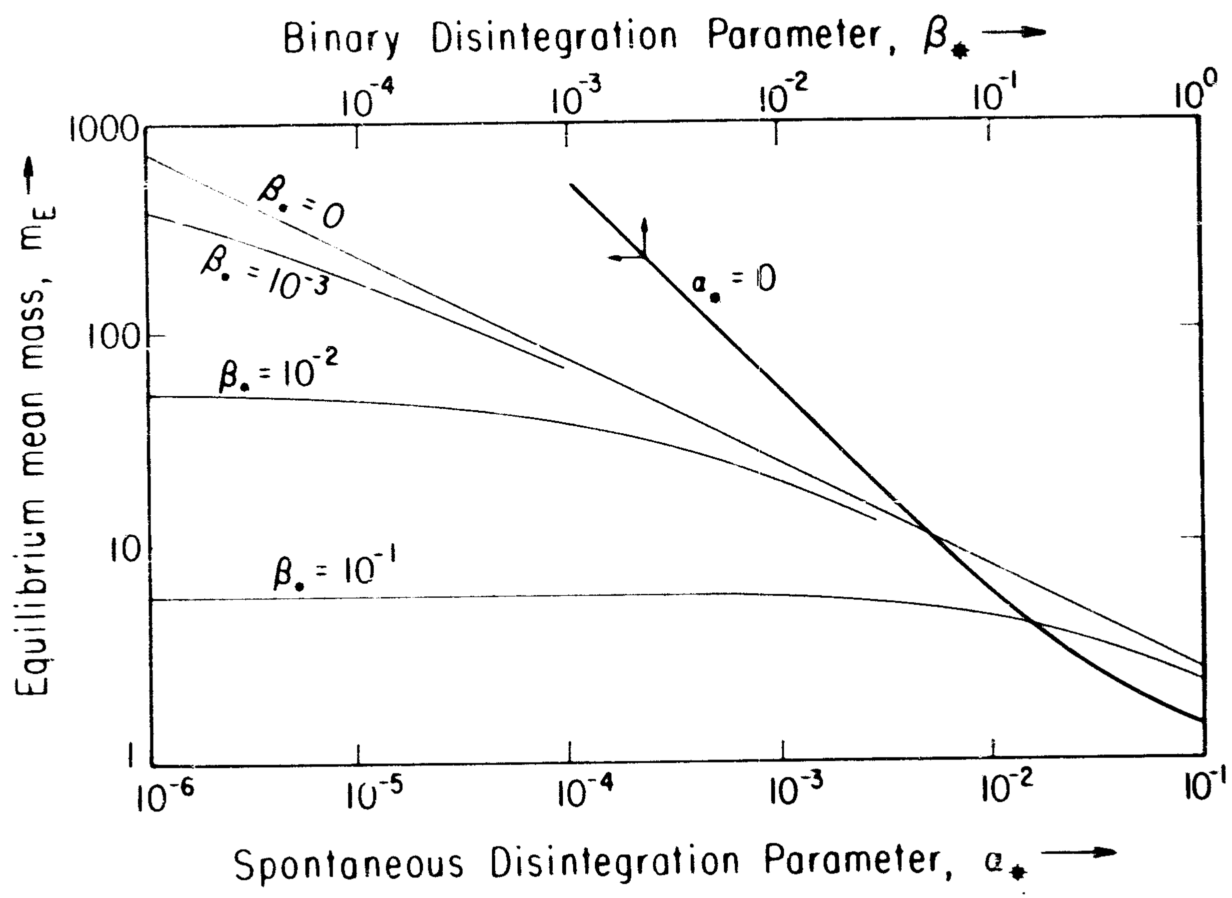

Figure 2. Variation of the equilibrium mean mass with the spontaneous and binary disintegration parameters.

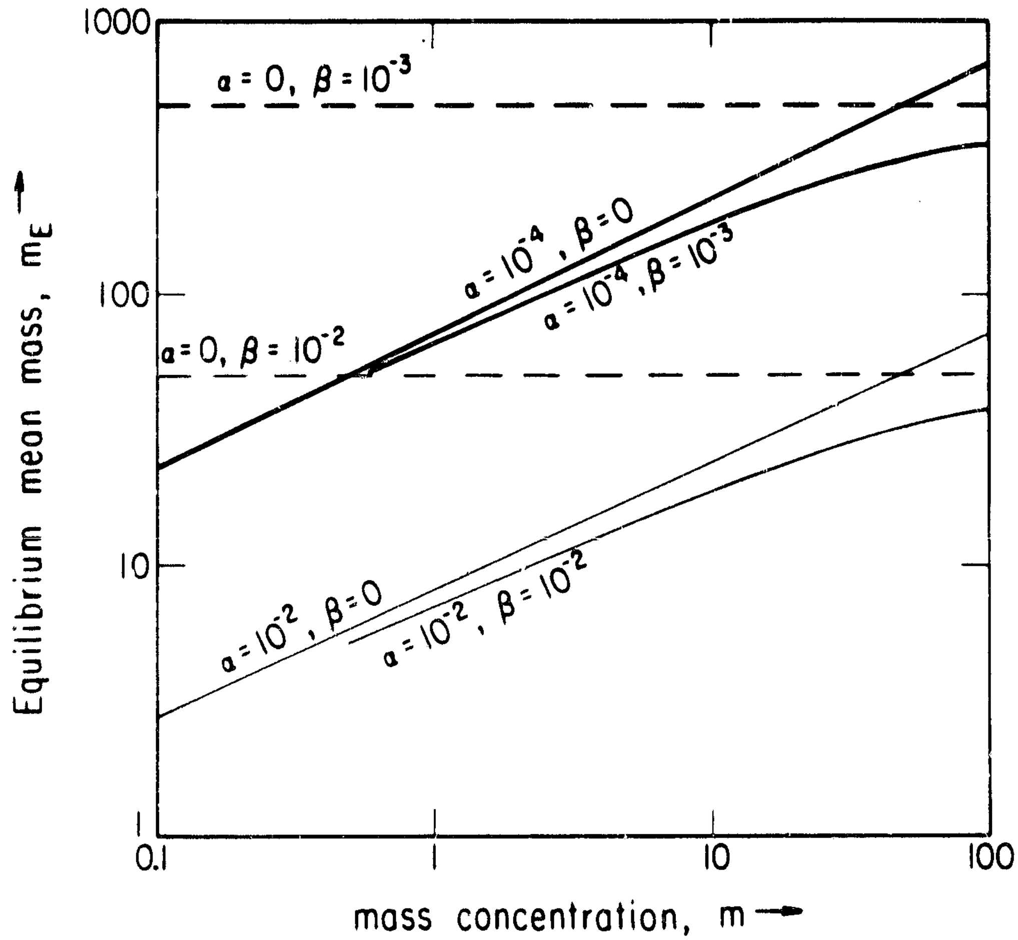

Figure 3. Variation of mean mass with total mass concentration for selected values of the disintegration parameters.

increases, however, the reverse is the case. A similar effect occurs for realistic formulations of collection and breakup of raindrops (Srivastava 1978).

3.1.2 Equilibrium Particle Size Distribution

The scaled equilibrium generating function is found by putting $\partial/\partial\tau = o$ in Equation (8):

$$g_E^2/2 - g_E\,(\alpha_* + \beta_*/m_E + 1/m_E) + (\alpha_* + \beta_*/m_E)z = o \tag{18}$$

considering the coefficients of z in (18) we find:

$$P_{1E} = (\alpha_* + \beta_*/m_E)\;/(\alpha_* + \beta_*/m_E + 1/m_E) \tag{19}$$

or, using Equation (17)

$$P_{1E} = 1/(2m_E-1) \tag{20}$$

Solving Equation (18) for g_E, differentiating the result repeatedly with respect to z, and putting z = 1, we find the following recursion equation for P_{kE}:

$$P_{kE}\;/\;P_{k-1,E} = \frac{2k-3}{2k} \cdot \frac{m_E^2 - m_E}{\left(m_E - 1/2\right)^2} \tag{21}$$

Equation (21) can also be written as:

$$P_{kE} = \frac{(2k-2)!}{k!\,(k-1)!}\;\frac{1}{2^{2k-1}}\;\frac{(m_E^2 - m_E)^{k-1}}{(m_E - 1/2)^{2k-1}}\;. \tag{22}$$

From Equation (22), it is seen that the equilibrium size distribution depends explicitly only on m_E. The dependence on the parameters α_* and β_* is implicit through the dependence of m_E on those parameters. In other words, the form of the equilibrium size distribution is the same for (i) coalescence and spontaneous disintegration, (ii) coalescence and binary disintegration, and (iii) coalescence, spontaneous and binary disintegration. Consideration of the particular forms of m_E shows further that in case (ii), the equilibrium distributions for given β_* and different M are parallel to each other, the particle concentrations being proportional to M. This is not so in cases (i) and (iii). This result is understandable. In the case of coalescence and binary disintegration, all terms in the equation for the equilibrium distribution are proportional to the products of particle concentrations. Therefore if one solution p_{kE} for a mass concentration M has been found, A p_{kE} is a possible solution for a mass concentration AM where A is a constant. In the case of coalescence and spontaneous breakup, however, the particle concentrations enter into the equation both linearly and quadratically and hence we do not anticipate size distributions which are parallel to each other. Gillespie and List (1978) and Srivastava (1978) found similar behavior with realistic formulations of coalescence and spontaneous and collisional breakup.

For large k, we can approximate P_{kE} in Equation (22) by

$$P_{kE} = \frac{(m_E - 1/2)}{(m_E^2 - m_E)} \left[\frac{m_E^2 - m_E}{(m_E - 1/2)^2} \right]^k k^{-3/2} \Big/ [2\pi]^{1/2} \qquad (23)$$

Lushnikov and Piskunov (1977) considered the problem of coalescence and spontaneous disintegration and obtained equations similar to our Equations (21), (22) and (23). Here we have shown that these results are also valid for coalescence and binary disintegration and a combination of coalescence, spontaneous and binary disintegration processes provided the appropriate m_E is used in Equations (20) through (23).

Fig. 4 shows a plot of the equilibrium distribution for $m_E = 50$, computed from Equation (22). Although indicated as a continuous curve, the distribution is discrete. On this figure, the asymptotic form (23) is indistinguishable from the exact solution for $k \geq 8$. For cloud physical purposes, it is perhaps more interesting to see the distributions plotted as log ($p_k \cdot k^{2/3}$) against $k^{1/3}$ (Fig. 5) which corresponds essentially

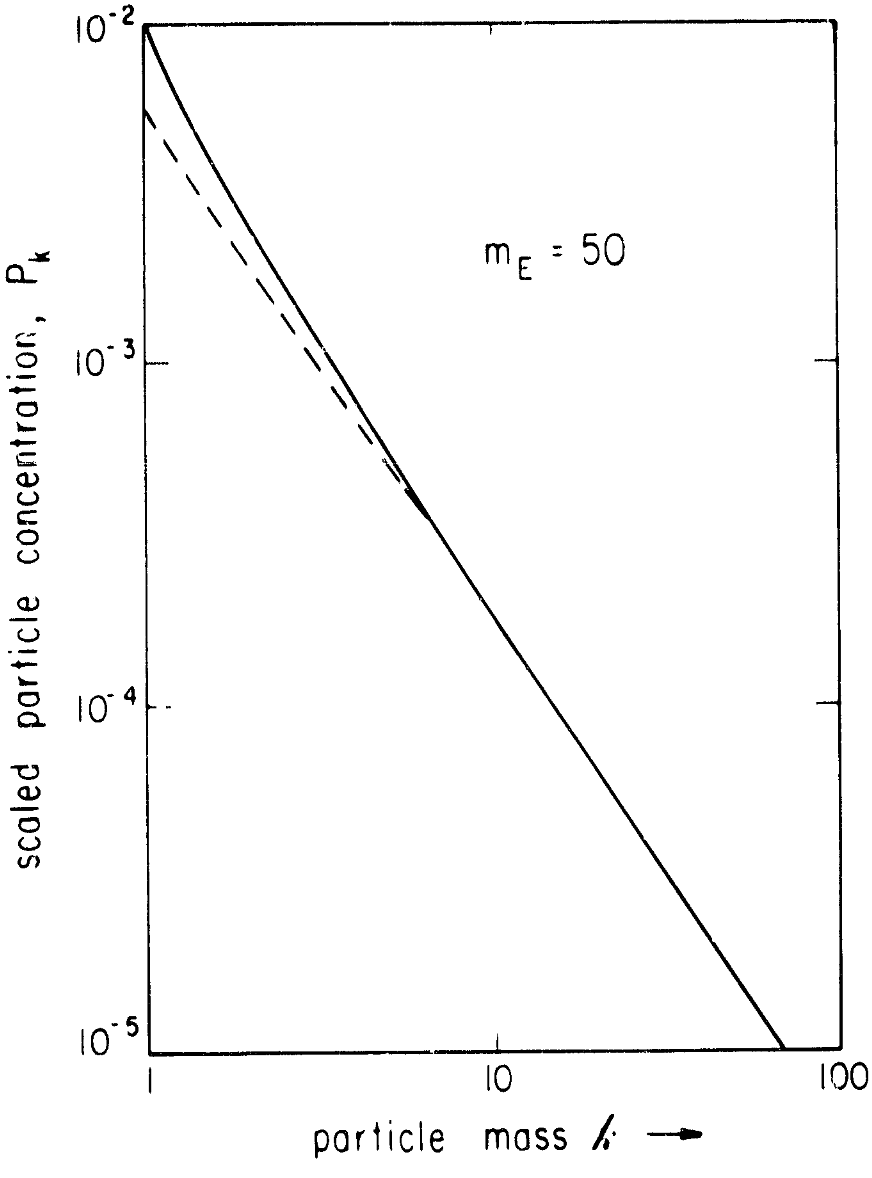

Figure 4. Scaled equilibrium size distribution (full line) for an equilibrium mean mass m_E = 50 compared with the asymptotic solution (dashed line).

to a plot of log N(D) vs D where D is the particle diameter and N(D) the particle concentration density. In Fig. 5, the scaling has been removed and the equilibrium distributions for coalescence and spontaneous breakup ($\alpha/c = 0.1$ $\beta = 0$) have veen shown for the indicated mass concentrations. Curves identical in form to those in Fig. 5 would be obtained for other cases provided the m_E are identical. As an example, let us consider the M = 2 curve in Fig. 4. This curve has $m_E = 3.70$ (Eq. 12). Under the action of coalescence and binary breakup, the same m_E would be obtained for $\beta/c = 0.185$ (Eq. 14). Hence the M = 2 curve in Fig. 5 is also the equilibrium distribution for coalescence and collisional breakup for $\beta/c = 0.185$, and M = 2. However, if M is changed with β/c kept fixed, the equilibrium distribution will be displaced parallel to itself.

3.2 Other forms of the collection kernel and breakup parameters.

Solutions have also been obtained for constant breakup parameters and (a) collection kernel proportional to the sum of particle masses and (b) collection kernel proportional to the product of particle masses. A detailed discussion of these solutions will not be given here. Only certain new features which emerge in the behavior of the particle mean mass are summarized below.

As the power of the collection kernel increases, an equilibrium mean mass is not always possible. In case (a), an equilibrium mean mass is always obtained with coalescence and spontaneous breakup. With coalescence and binary breakup, however, an equilibrium M occurs only for $\beta_* > 1$ and the equilibrium value is independent of the mass content M. For $\beta_* < 1$, coalescence dominates, that is $m \rightarrow \infty$ as $\tau \rightarrow \infty$.

In cases (b), m exhibits three distinct kinds of behavior. In a region of relatively large α_* and β_* an equilibrium m is always attained. In a region of small α_* and β_*, coalescence dominates in a finite time τ_c,

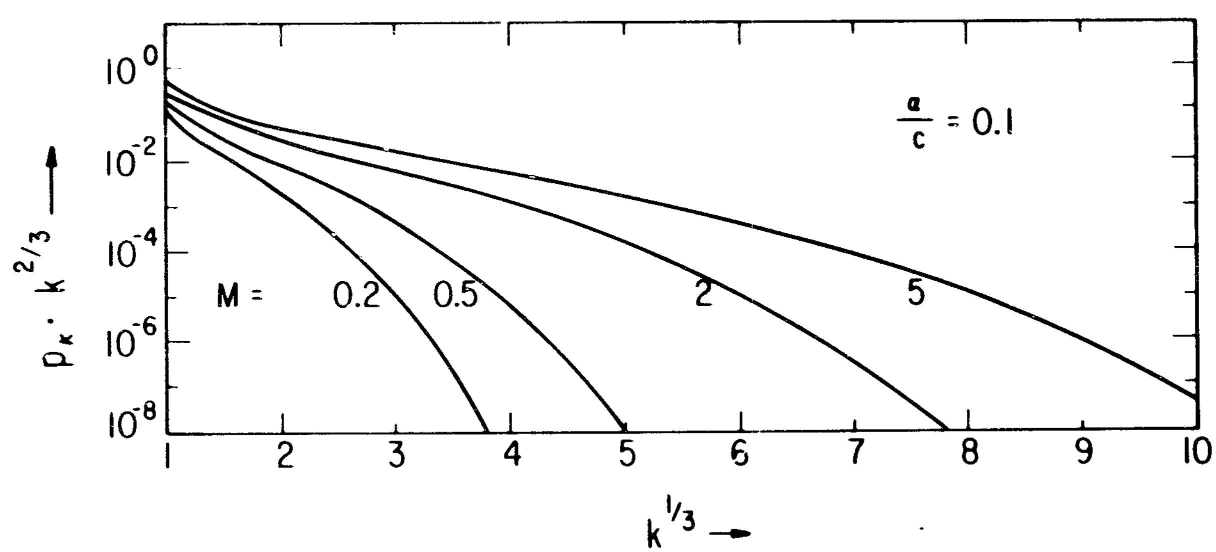

Figure 5. Equilibrium size distribution, for selected mass concentrations, under the action of coalescence and spontaneous breakup.

i.e., $m \to \infty$ as $\tau \to \tau_c$. In a third region of small α_* but relatively large β_*, the behavior of m depends upon the initial condition. For small initial m an equilibrium m is attained while for large initial m, coalescence dominates. Moreover, two equilibrium values of m are possible. The smaller m is stable with respect to small perturbations, while the equilibrium point with the larger m is unstable. In the latter case, a small positive perturbation causes coalescence to dominate while a small negative perturbation causes the m to move to the stable equilibrium point. In this case also the equilibrium m is independent of M for coalescence and binary breakup.

Besides the above, it is also possible to obtain solutions for certain forms of variable breakup parameters. For example, we can consider

$$K(j,k) = cjk$$

$$\alpha(k) = \alpha_o k$$

$$\beta(j,k) = \beta_o jk$$

where c, α_o and β_o are constants. A reference to Equations (1) will show that in this case, at equilibrium, the quantity jp_j obeys the same equation as the quantity p_j in the case of a constant kernel and breakup parameters. Hence the solution to this problem is immediate.

4. CONCLUSIONS

The equations for a simple model of particle coalescence and breakup have been formulated. Analytical solutions of the equations have been obtained for a constant collection kernel and constant spontaneous and binary disintegration parameters. The behavior of the solutions is qualitatively similar to that of numerical solutions of the equations for the evolution of raindrop size distributions for realistic formulations of coalescence and breakup. An equilibrium particle size distribution is attained. For given breakup parameters, the effect of spontaneous disintegration dominates over that of binary disintegration at small mass contents, M, while the reverse is the case at large M. With coalescence and only spontaneous disintegration, the equilibrium mean mass m_E increases with M while it is independent of M when coalescence and only binary disintegration are considered. In the latter case, the equilibrium particle size distributions for different M are parallel to each other.

ACKNOWLEDGEMENTS: The research reported here was supported by grants NASA-NSG-5402 and NSF-ATM-80-16150. I wish to acknowledge the help of Mr. Tim Lorello in the calculations. Thanks are due to Ms. Carolyn Gay for typing the manuscript of the paper.

REFERENCES:

Gillespie, J.R. and R. List, 1978: Effects of Collision-induced Breakup on Drop Size Distributions in Steady Rain Shafts. Pageoph, 117, 599-626.

Lushnikov, A.A., and V.N. Piskunov, 1977: Formation of Steady-State Distributions in Coagulating Systems with Disintegrating Particles. Colloid Journal, 39, 760-764.

Scott, W.T., 1968: Analytic Studies of Cloud Droplet Coalescence. J. Atmos. Sci., 25, 54-65.

Srivastava, R.C., 1971: Size Distribution of Raindrops Generated by their Breakup and Coalescence. J. Atmos. Sci., 28, 410-415.

Srivastava, R.C., 1978: Parameterization of Raindrop Size Distributions. J. Atmos. Sci., 35, 108-117.

Young, K.C., 1975: The Evolution of Drop Spectra due to Condensation, Coalescence and Breakup. J. Atmos. Sci., 32, 965-973.

DOPPLER RADAR STUDY OF A REGION OF WIDESPREAD
PRECIPITATION TRAILING A MID-LATITUDE SQUALL LINE

by

Thomas J. Matejka and Ramesh C. Srivastava

Department of Geophysical Sciences
The University of Chicago
Chicago, Illinois 60637

25 July 1981

DOPPLER RADAR STUDY OF A REGION OF WIDESPREAD PRECIPITATION TRAILING A MID-LATITUDE SQUALL LINE

Thomas J. Matejka and Ramesh C. Srivastava
Department of Geophysical Sciences
The University of Chicago
Chicago, Illinois

1. INTRODUCTION

Long-lived intense squall lines are sustained and propagated by the initiation of new convection on their leading faces. As the thunderstorms associated with the new convection mature and dissipate, they move to the rear of the propagating line. Under certain conditions not well understood at the present time, the anvils and debris associated with the dissipating thunderstorms can merge together to produce a large mesoscale region (area $\approx 10^4$ km^2) of deep and relatively homogeneous precipitation which trails the line of active convection. Such squall lines have been described by Zipser (1969, 1977) and Houze (1977).

Observations and theoretical considerations suggest that the region of trailing precipitation may be dynamically active and contain mesoscale vertical air motions. This is suggested by the long life of the region and the fact that it sometimes accounts for a large fraction (≈ 0.4) of the total precipitation of the squall line system (Houze, 1977). Physically, it can be seen why vertical motions occur in the region of widespread precipitation if conditions are favorable for evaporation in the lower layers; the cooling associated with the evaporation (perhaps augmented by the melting of ice) can give rise to pressure falls and convergence in the middle troposphere, which should result in ascent in the upper levels and descent in the lower levels. The ascent could lead to the production of more precipitation and perhaps a self-sustaining system.

In this paper, we present Doppler radar observations of a region of widespread precipitation trailing an intense squall line. The observations were obtained during Project NIMROD, conducted in Illinois during May and June 1978. Three Doppler radars (the NCAR CP3 and CP4 and the University of Chicago - Illinois State Water Survey CHILL) were used besides surface instrumentation (the NCAR PAM system and the ISWS raingauge network) and frequent rawinsonde ascents. Here we shall present observations from only one radar (CP3), which were used to calculate high-resolution vertical profiles of particle fall speed, horizontal divergence, and vertical velocity by a modest extension of the VAD method (Browning and Wexler, 1968).

2. BRIEF DESCRIPTION OF THE SQUALL LINE

The band of intense precipitation from the squall line, followed by the region of light, widespread precipitation, passed through northern Illinois between 2200 CDT (all times are Central Daylight Time), 17 June and 0200, 18 June 1978.

Fig. 1a is a PPI display of radar reflectivity factor at 2215 and shows the squall line at a stage when the widespread precipitation to the rear of the active line was just beginning to become extensive. By 2346, the convective line had weakened considerably, and the area of widespread precipitation had enlarged, extending aloft behind the line for a distance of 140 km (Fig. 1b). By this time also the line of intense activity had become detached from the area of intense precipitation by a gap of over 20 km (Fig. 1b). Since light, widespread precipitation continued for two more hours, the existence of mesoscale ascent to provide additional condensate seems likely.

3. EXTENDED METHOD OF VAD ANALYSIS

In a region of horizontally stratified precipitation with linear variations of the horizontal wind, the Doppler radial velocity at a constant elevation angle α, and constant slant range R (horizontal range r) is related to the azimuth angle ϕ (measured clockwise from north) by the equation (Browning and Wexler, 1968)

$$V = a_o + a_1\cos\phi + a_2\sin\phi + b_1\cos 2\phi + b_2\sin 2\phi \quad (1)$$

where

$$a_o = \frac{r\cos\alpha}{2}\,\mathrm{Div} - F\sin\alpha \quad (2)$$

$$a_1 = v\cos\alpha\ ,\ a_2 = u\cos\alpha\ , \quad (3)$$

Here Div is the average divergence of the horizontal wind over the area of the VAD circle, F is the average particle fall speed (positive downwards) over the circumference of the VAD circle, and u and v are respectively the eastward and northward components of the wind velocity over the radar. The coefficients b_1 and b_2 in (1) are related to the deformation of the horizontal wind and will not be used here. The usual practice in VAD analysis has been to take observations of V, as a function of the azimuth ϕ, at one elevation angle and to calculate the coefficients a_o, a_1, a_2, b_1, b_2 either by harmonic analysis of the $\hat{V}(\phi)$ or by a least-squares fitting procedure. Observations in different range bins, corresponding to different R (and thus having different r and height h), then give the height profiles of the coefficients. The coefficient a_o can be used to determine the vertical profile of horizontal divergence, and thence by integration the profile of the vertical air velocity w, provided F is known or the elevation angle α is small enough to neglect the last term in Equation (2); in most previous work, α was kept small so that the latter was the case.

Here we have extended the VAD method, so that observations of $V(\phi)$, at a number of elevation angles, can be used to deduce both the divergence and the fall speed, and it is not necessary (in fact, it is not desirable) to restrict the VAD scans to small elevation angles.

Let us rewrite Eq. (2) as follows:

$$\frac{2a_o}{r\cos\alpha} = \mathrm{Div} - 2F\,\frac{\tan\alpha}{r} \qquad (4)$$

The VAD scans at different elevation angles can be used to determine the a_o's and the quantity on the left hand side of (4) for the range gates that fall into a narrow height interval. The

(a)

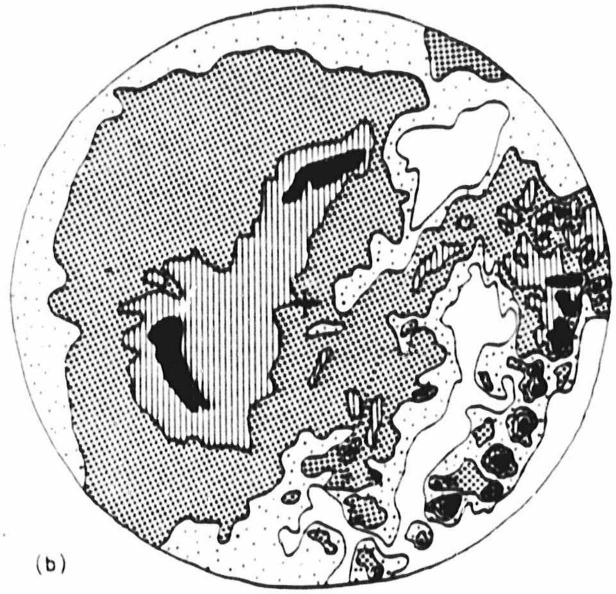

(b)

Fig. 1. PPI displays of CP-3 radar reflectivity factor. Black >40, hatched 30-40, densely stippled 20-30, sparsely stippled <20 dBZ. Cross indicates position of radar. Maximum range is 108 km. (a) 2215 CDT; elevation 4.5°; squall line is to northwest. (b) 2346 CDT; elevation 3.5°; squall line is far to southeast. In (b), maxima 50 km to the north and southwest are associated with the melting band.

left hand side of (4) then has a distinctive dependence on α which can be used to seperate the Div and F. Besides requiring the assumptions made in the usual VAD analysis (viz., horizontal uniformity of precipitation and linear variations of the winds in horizontal layers), the present method is more stringent in terms of requiring temporal uniformity of the phenomenon because many VAD scans must be utilized in the analysis procedure. However, the method does contain an internal test of consistency through the requirement of an explicit dependence of $(a_o/r\cos\alpha)$ on α.

In the present analysis, data from 21 complete azimuthal scans, ranging in elevation angle from 0.5° to 84.5°, have been used. The time period for these radar scans was from 2345 to 2355. Each azimuthal scan had approximately 470 observations of Doppler velocity. Only the data for the range bins within $r \leq 40$ km of the radar were utilized.

The data were first edited to remove "clutter" points (absolute value of radial velocity less than 1 ms^{-1}) and velocities which were observed in the antenna's side lobe due to "shadowing" effects. The radial velocities were unfolded by comparison with the hodograph from a rawinsonde ascent at 2356 CDT from the CP3 radar site. A first fit of type (1) was made by a least-squares method for each azimuthal scan and range bin subject to the range constraint mentioned above. (Approximately 2500 fits were made.) The Doppler velocities were then "cleaned" by removing velocities which deviated from the fit by more than twice the standard error of the first fit. The "cleaning" had the effect of removing spurious observations rather than meteorologically significant data. A second least-squares fit was then made on the "cleaned" points to determine the coefficients in (1) for each elevation angle and range bin.

The next analysis step consisted of stratifying the a_o's in narrow height intervals (500m). A least squares fit, according to Eq. (4), was performed to determine Div and F for each of the layers. An integration was then carried out to determine the vertical air velocity. The details of this are described later.

For the sake of brevity, we have omitted, in the above, certain details of the analysis procedures. These are: (i) height and elevation angle correction for ray-curvature (the latter correction was a small fraction of a degree at the farthest range considered) and (ii) an extension of the fit of Eq. (4) to include quadratic height variations of Div and F within a layer; this was done to account better for sharp variations, such as through the melting layer.

4. DISCUSSION OF RESULTS

4.1 Winds, temperature, and humidity

Vertical profiles of wind speed and direction obtained from the VAD analysis in the region of widespread precipitation behind the squall line and from a rawinsonde launched from the CP3 radar site at 2356 are shown in Fig. 2. Vertical profiles of temperature and dew-point temperature are also shown.

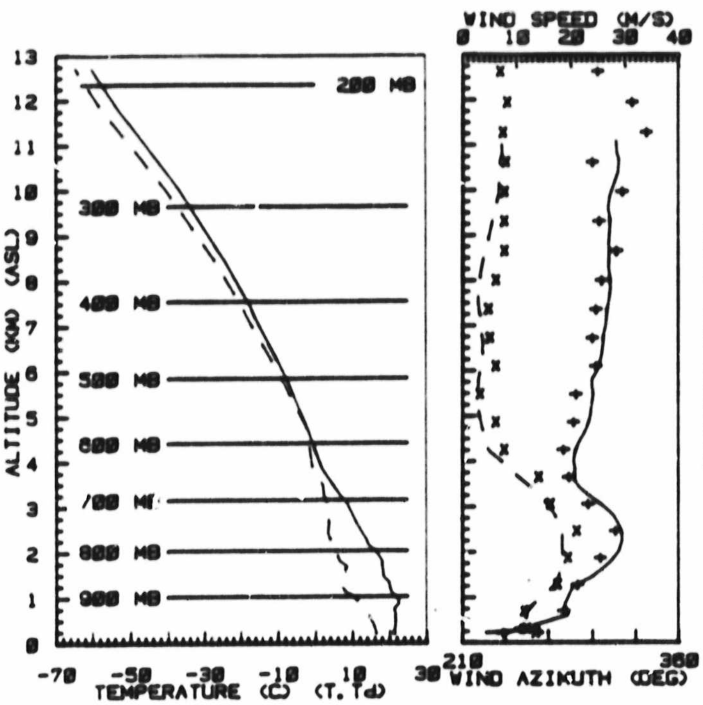

(a) (b)

Fig.2. (a) Vertical profiles of temperature (solid line) and dew-point temperature (dashed line) from rawinsonde sounding. (b) vertical profiles of wind direction (solid line) and wind speed (dashed line) from the VAD analysis; also from rawinsonde sounding (+ and x). The vertical axis is altitude above sea level. Ground level was 226 m.

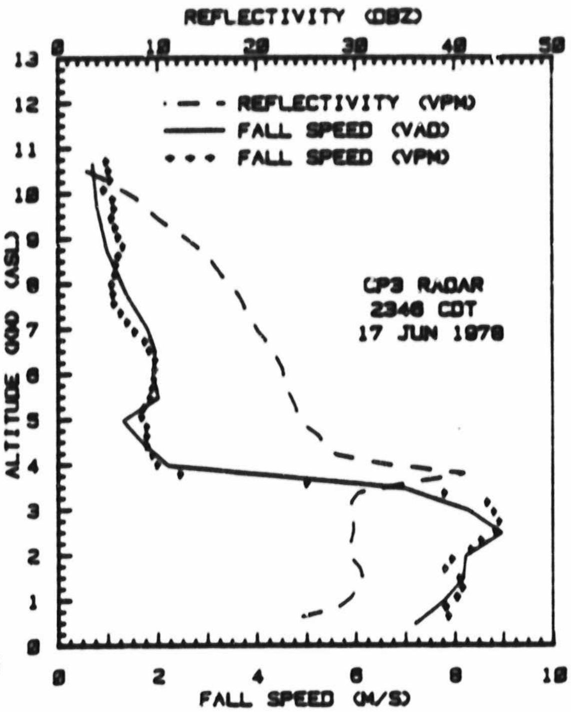

Fig. 3. Vertical profiles of hydrometeor fall-speed from the VAD analysis (solid line) and from radar data collected in vertically-pointing mode (VPM) (+) and of radar reflectivity factor from VPM (dashed line).

The thermal structure of the atmosphere resembled the soundings behind tropical lines described by Zipser (1977) and behind an Oklahoma squall line described by Ogura and Liou (1980). Below 4 km, the sounding was consistent with the occurrence of evaporation of precipitation and unsaturated descent (Leary, 1980). Above 4.0 km, the atmosphere was saturated with respect to ice. Between 4.0 and 8.7 km and above 11.0 km, the atmosphere was stable. Between 8.7 and 11.0 km, it was conditionally unstable. The layer from the surface to about 1 km was very stable. The wet bulb potential temperature in this layer was 292 K. In the layer from 1 to 4 km it was mostly between 290.5 and 291.5. This contrast supports Zipser's (1977) conclusion that the air in these two layers has different origins.

4.2 Hydrometeor fall speed and reflectivity factor

The vertical profile of hydrometeor fall speed obtained from our extension of the VAD method is shown in Fig. 3. The profiles of average fall speed and reflectivity factor measured while the radar was in the vertically pointing mode during the 5.5 min immediately following the VAD scans are also shown. The two sets of fall speeds are in good agreement; especially noteworthy is the agreement through the sharp transition in the melting zone between the altitudes of about 3 and 4 km. This agreement supports our method of separating the fall speed and divergence from the "average" of the VAD velocities (a_o) and also gives credence to the assumptions underlying the use of the method.

From 11 km down to 6.5 km, the fall speeds generally increased from 1 to 2 ms^{-1}. These fall speeds are typical of snow. The increase of the fall speed and of the reflectivity factor imply the occurrence of particle growth by some or all of the following processes: deposition, riming and aggregation. Between 6.5 and 4.2 km, the increase of fall speed was arrested, and the rate of increase of reflectivity factor also diminished. The former could have been due to the formation of large aggregates, whose fall speeds are a very weak function of their mass. The latter could perhaps have been due to the cessation of some of the growth processes operative above 6.5 km.

The fall speeds increased rapidly from about 2 to 9 ms^{-1} in the melting region and then decreased downwards to approximately 7.5-8 ms^{-1}. The reflectivity factor increased sharply from about 28 to 41 dBZ and then fell again to 29 dBZ. This implies a preponderance of considerable particle aggregation above, and break-up below, the peak of the reflectivity curve. The peak fall speed of about 9 ms^{-1} was unusually high for a melting-band situation. It implies the existence of rather massive particles in the forms of aggregates or rimed particles; these particles

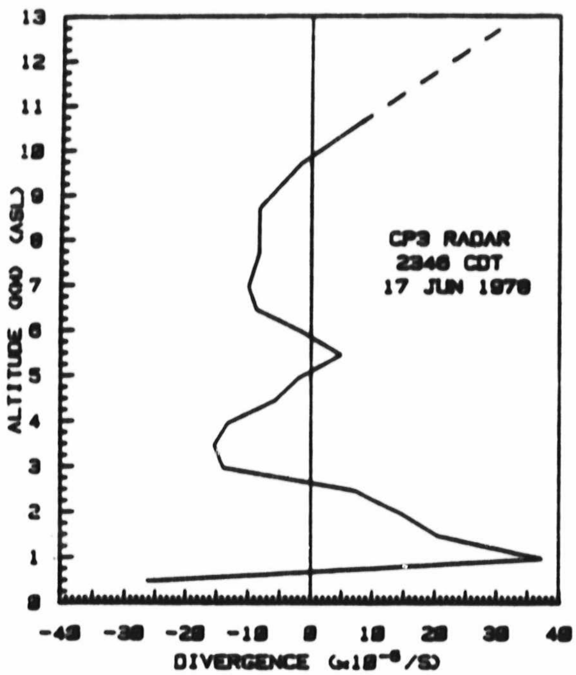

Fig. 4. Vertical profile of horizontal divergence from VAD analysis. The dashed line represents an extrapolation of the profile to cloud top.

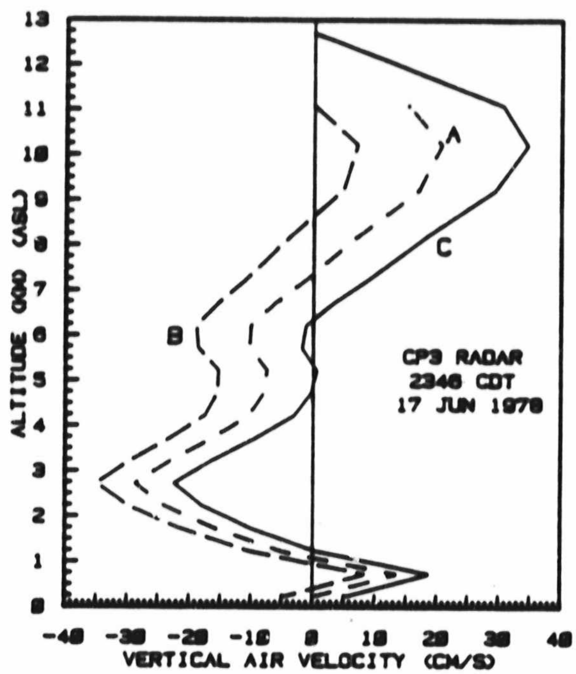

Fig. 5. Vertical profiles of vertical air velocities, computed from integrations of the divergence profile (Fig. 4).

could even have been derived from the debris of the intense convection. The decrease of the fall velocity to ≈ 7.5-8 ms^{-1} in lower levels is consistent with continued particle breakup and raindrop size distributions having the measured reflectivity factors.

4.3 Horizontal divergence and vertical air velocity

The vertical profile of the horizontal divergence obtained from the VAD analysis is shown in Fig. 4. A discrete form of the approximate continuity equation

$$Div + \partial(\rho w)/\partial h = 0$$

was integrated to obtain the vertical air velocity w. The air density ρ was taken from the rawinsonde ascent. Three alternative boundary conditions gave the three vertical air velocity profiles shown in Fig. 5. For curve (A), w was taken to be 0 at ground level. This was justified by the observed low-level winds and the known terrain of the area. Curve (B) was obtained by assuming that w = 0 at h = 11.1 km, the top of the radar data used to obtain the divergence profile. Above this height, the radar data were spotty, and it was difficult to calculate a reliable value of the horizontal divergence. However, the cloud did extend above this level. This is supported by the presence of upward motion at this height in curve (A) and by satellite data. The cloud top was estimated to be at h = 12.7 km from infrared satellite imagery. The third integration therefore assumed w = 0 at h = 12.7 km and produced curve (C) of Fig. 5. For this integration, the divergence profile of Fig. 4 was extrapolated linearly to higherlevels, giving Div = $3.1 \times 10^{-4} s^{-1}$ at h = 12.7 km. (This extrapolation is shown by the dashed line in Fig. 4) At this time, we believe profile (C) to be nearer the actual vertical motion than either of the other profiles. It may be remarked here that small changes in the assumed boundary condition at a low level give large changes in the integrated w at high levels, while small changes in the assumed boundary condition at a high level give rise to only small changes in the computed w at low levels (Bohne and Srivastava, 1976).

The maximum convergence, $-1.5 \times 10^{-4} s^{-1}$, occurred at h ≈ 3.5 km in the melting zone. Above 3.5 km, the wind field was convergent up to h ≈ 9.9 km, above which it became rapidly divergent. Below 3.5 km, the convergence changed very rapidly to a strong divergent field through the melting layer with a maximum divergence of about $4 \times 10^{-4} s^{-1}$ at 1.0 km. In the 270 m layer nearest the ground, the wind field again became convergent. This result was also indicated by an objective analysis of PAM network observations, which yielded a convergent wind field although of much smaller magnitude, $-3 \times 10^{-5} s^{-1}$.

The vertical velocity profiles show that the troposphere was characterized by a deep layer of descent below and a deep layer of ascent above. A maximum downward velocity of -25 to -35 cm s^{-1} occurred at h ≈ 3 km. From near the 0C level (h ≈ 3 km) to about 7 km height, the computed vertical motions are small (≈ 10 cm s^{-1}) and perhaps near the limits of accuracy of the analysis. Above 7 km, ascent occurred with a maximum of between 10 and 35 cm s^{-1}. The profiles are consistent with Zipser (1977), who concluded that the mesoscale downdraft air penetrates to within 1 km of, but does not reach, the surface.

The computed profiles of vertical air velocity are consistent with the profiles of temperature and dew-point temperature, i.e., the region of descent was unsaturated, while the region of ascent was near saturation.

The profiles of divergence and vertical air velocity are remarkably consistent with the profiles of these quantities postulated, or deduced from indirect evidence, by Zipser (1969, 1977) and Houze (1977) for the region of widespread precipitation behind tropical squall lines. Ogura and Liou (1980) analyzed radiosonde data for an Oklahoma squall line and obtained profiles of divergence and vertical air velocity in the rear portions of the squall line very similar to those obtained here. A numerical model (Brown, 1979) of the region of widespread precipitation, with parameterization of the intense convection, also yielded areas of upward and downward air motions of similar intensity and distribution in height.

5. SUMMARY AND CONCLUDING REMARKS

An extension of the VAD method has been developed which enables the calculation of high-resolution vertical profiles of particle fall speed and horizontal divergence (and, therefore, the vertical air velocity). The method utilizes azimuthal scans of Doppler velocity at a number of elevation angles. The method has been applied to the study of a region of widespread precipitation trailing an intense squall line during Project NIMROD. The extended VAD analysis gave vertical profiles of particle fall speed in excellent agreement with the profiles obtained by vertically pointing observations, even through the region of sharp changes in the melting layer. The computed vertical air velocities showed general descent below the 0C isotherm, general ascent above h ≈ 7 km, and small vertical air motions in the intermediate layer. The profile of vertical air velocity is consistent with what has been deduced to occur behind tropical squall lines and in an Oklahoma squall line from indirect evidence and from radiosonde observations, respectively. This study gives the first direct evidence of the vertical air velocities in the region of widespread precipitation associated with a squall line.

Quantitative knowledge of the characteristics of the region of widespread precipitation is important for a number of reasons. In this study we obtained vertical air motions of order 10 cm s^{-1} over the analyzed area of radius 40 km (the actual area could be larger). The transports effected by such ascent are equivalent to the transports which would be effected by 16 elements each of radius 1 km having a vertical air velocity of 10 ms^{-1}. Hence the mesoscale vertical motions in the region behind the active convection in the squall line cannot be ignored in considerations of budgets of the squall line. The vertical motions could also have dynamical significance for the life history of the squall line.

ACKNOWLEDGEMENTS

The research reported here was supported by the Atmospheric Sciences Section of the National Science Foundation (ATM-80-16150) and by the National Aeronautics and Space Administration (NSG-5402). The Field Observing Facility, NCAR, operated the CP3, CP4 radars and the Portable Automated Meso-network during Project NIMROD. The computations were performed on the CDC-7600 computer at the National Center for Atmospheric Research and this laboratory's minicomputer. Mr. Tim Lorello helped in the development and execution of most of the computer programs used in this research. The manuscript was expertly typed by Ms. Carolyn Gay.

REFERENCES

Bohne, A.R., and R.C. Srivastava, 1976: Random errors in wind and precipitation fall speed measurement by a triple Doppler radar system. Preprints, 17 Conf. on Radar Meteor., Amer. Meteor. Soc., Boston, MA, 7-14.

Brown, J.M., 1979: Mesoscale unsaturated downdrafts driven by rainfall evaporation: a numerical study. J. Atmos. Sci., 36, 313-318.

Browning, K.A. And R. Wexler, 1968: A determination of kinematic properties of a wind field using Doppler radar. J. Appl. Meteor., 7, 105-113.

Houze, R.A., Jr., 1977: Structure and dynamics of a tropical squall-line system. Mon. Wea. Rev., 105, 1540-1567.

Leary, C.A., 1980: Temperature and humidity profiles in mesoscale unsaturated downdrafts. J. Atmos. Sci., 37, 1005-1012.

Ogura, Y., and M.-T. Liou, 1980: The structure of a midlatitude squall line: a case study. J. Atmos. Sci., 37, 553-567.

Zispar, E.J. 1969: The role of organized unsaturated convective downdrafts in the structure and rapid decay of an equitorial disturbance. J. Appl. Meteor., 8, 799-814.

________. 1977: Mesoscale and convective scale downdrafts as distinct components of squall line structure. Mon. Wea. Rev., 105, 1568-1589.